

# X-ray flares on zero-age- and pre-main sequence stars in Taurus-Auriga-Perseus

B. Stelzer<sup>1</sup>, R. Neuhäuser<sup>1</sup> and V. Hambaryan<sup>2</sup>

<sup>1</sup> Max-Planck-Institut für extraterrestrische Physik, Giessenbachstr. 1, D-85740 Garching, Germany

<sup>2</sup> Astrophysikalisches Institut Potsdam, An der Sternwarte 16, D-14482 Potsdam, Germany

Received <6 April 1999> / Accepted <3 February 2000>

**Abstract.** We present the results of a systematic search for X-ray flares on young stars observed during *ROSAT* PSPC observations of the Taurus-Auriga-Perseus sky region. All pointed PSPC observations currently available from the *ROSAT* Public Data Archive with known pre-main sequence T Tauri Stars or young Pleiads or Hyads in the field of view are analyzed. A study of the activity of late-type stars of different ages provides information on the evolution of their coronal activity, which may be linked to their angular momentum.

We develop a criterion for the detection of flares based on the shape of the X-ray lightcurve. Applying our detection method to all 104 PSPC pointings from the archive we find 52 flares. Among them 15 are detected on T Tauri Stars, 20 on Pleiads, and 17 on Hyads. Only the 38 events which can definitely be attributed to late-type stars (i.e. stars of spectral type G and later) are considered in the statistical analysis of the properties of flaring stars. We investigate the influence of stellar parameters such as age, rotation and multiplicity on individual flare parameters and flare frequency.

From the total exposure time falling to the share of each sample and the duration of the individual flares we compute a flare rate. We take into account that the detection sensitivity for large X-ray flares depends on the S/N and hence on the stellar distance. The values we derive for the flare rates are  $0.86 \pm 0.16\%$  for T Tauri Stars,  $0.67 \pm 0.13\%$  for Pleiads and  $0.32 \pm 0.17\%$  for Hyads. The flare rate of classical T Tauri Stars may be somewhat higher than that of weak-line T Tauri Stars ( $F_c = 1.09 \pm 0.39\%$  versus  $F_w = 0.65 \pm 0.16\%$ ).

Hardness ratios are used to track the heating that takes place during stellar flares. Hardness ratios are evaluated for three distinct phases of the flare: the rise, the decay, and the quiescent (pre- and post-flare) stage. In most cases the hardness increases during the flares as compared to the quiescent state. During both quiescence and flare phase TTSs display the largest hardness ratios, and the Hyades stars show the softest spectrum.

**Key words:** stars: flare – X-rays: stars – stars: late-type

## 1. Introduction

The Taurus-Auriga-Perseus region offers the opportunity to study the X-ray emission of young stars at several evolutionary stages. The youngest stars observed by *ROSAT* in this portion of the sky are the T Tauri Stars (TTSs) of the Taurus-Auriga and Perseus star forming regions, late-type pre-main sequence (PMS) stars of  $M \leq 3M_\odot$  with an estimated age of  $10^5 - 10^7$  yrs. Two young star clusters, the Pleiades and Hyades, are also located in this region of the sky at age of  $10^8$  yrs and  $6 \cdot 10^8$  yrs, respectively. They consist mostly of zero-age main-sequence (ZAMS) stars, except for some higher mass post-main sequence stars and brown dwarfs, which are not studied here.

From the early observations by the *Einstein* satellite it was concluded that the X-ray emission of young stars arises in an optically thin, hot plasma at temperatures above  $10^6$  K (Feigelson & DeCampli 1981). The emission region has been associated with the stellar corona where the X-rays are produced — more or less analogous to the solar X-ray emission — through a stellar  $\alpha$ - $\Omega$ -dynamo. The dynamo is driven by the combination of rotation and convective motions. Correlations between the X-ray emission of late-type stars and the stellar rotation support the notion that dynamo-generated magnetic fields are responsible for heating the coronae (Pallavicini et al. 1981). But successful direct measurements of the magnetic fields of TTSs have been performed only recently (see e.g. Guenther et al. 1999). The details of the heating mechanism are still not well understood.

The correlation between stellar rotation and X-ray emission of late-type stars suggests that the rotational evolution of young stars determines the development of stellar activity. The rotational evolution of low-mass PMS stars partly depends on the circumstellar environment. While classical TTSs (hereafter cTTSs) are surrounded by a circumstellar disk, inferred from IR dust emission (Bertout et al. 1988, Strom et al. 1989, and Beckwith et al. 1990) and more recently from direct imaging (e.g. McCaughrean & O'Dell 1996), weak-line TTSs (wTTSs) lack such a disk, or at least the disk is not optically thick. Owing to contraction wTTSs spin up as they approach the main sequence. For cTTSs, on the other hand, coupling between the disk and the star may prevent spin-up (Bouvier et al. 1993). The

period observed on the ZAMS depends on the time the star has spent in the cTTS phase. After the main-sequence is reached, the rotation rate decreases again (see Bouvier et al. 1997a). As a consequence of their slower rotation, stars on the ZAMS and main sequence (MS) should on average show less X-ray activity than PMS stars.

Earlier investigations of X-ray observations of young late-type stars were mostly concerned with the quiescent emission (see Neuhäuser et al. 1995, Stauffer et al. 1994, Gagné et al. 1995, Hodgkin et al. 1995, Micela et al. 1996, 1999, Pye et al. 1994, and Stern et al. 1994). In contrast to these studies we focus on the occurrence of X-ray flares. Furthermore we discuss a larger sample than most of the previous studies by using *all* currently available observations from the *ROSAT* Public Data Archive that contain any TTS, Pleiad or Hyad in the field of view.

X-ray flares may be used as a diagnostics of stellar activity. They are thought to originate in magnetic loops. In contrast to findings from quasi-static loop modeling, the only direct determination of the size of a flaring region (Schmitt & Favata 1999) shows that the emitting region is very compact. In the loops which confine the coronal plasma magnetic reconnection suddenly frees large amounts of energy which is dissipated into heat and thus leads to a temporary enhancement of the X-ray emission. The decay of the lightcurve is accompanied by a corresponding (exponential) decay of the temperature and emission measure, which are obtained from one- or two-temperature spectral models for an optically thin, thermal plasma (Raymond & Smith 1977, Mewe et al. 1985, 1986).

The most powerful X-ray flares have been observed on the youngest objects, notably a flare on the infrared Class I protostar YLW 15 in  $\rho$  Oph which has been presented by Grosso et al. (1997). X-ray flares on TTSs observed so far (see Montmerle et al. 1983, Preibisch et al. 1993, Strom & Strom 1994, Preibisch et al. 1995, Gagné et al. 1995, Skinner et al. 1997, Tsuboi et al. 1998) exceed the maximum emission observed from solar flares by a factor of  $10^3$  and more. Some extreme events have shown X-ray luminosities of  $\sim L_x = 10^{33}$  erg/s. Although some of the strongest X-ray flares ever observed were detected on TTSs to date no systematic search for TTS flares was undertaken.

This paper is devoted to a study of the relation between X-ray flare activity and other stellar parameters, such as age, rotation rate, and multiplicity. For this purpose we perform a statistical investigation of *ROSAT* observations. We develop a method for the flare detection based on our conception of the typical shape of a flare lightcurve, where the term ‘typical shape’ refers to the characteristics of the X-ray lightcurve described above, i.e. a significant rise and subsequent decay of the lightcurve to the previous emission level. The database and source detection is described in Sect. 2. In Sect. 3 we describe how the lightcurves are generated. Our flare detection algorithm is explained in Sect. 4, where we also present all flare parameters derived from the X-ray lightcurves. Then we describe the influence of observational restrictions on the data analysis and how the related biases can be overcome (Sect. 5).

In Sect. 6 we compare the flare characteristics of different samples of flaring stars selected by their age, rotation rate, and multiplicity. We present luminosity functions for TTSs, Pleiads, and Hyads during flare and quiescence. Luminosity functions of the non-active state of these stars have been presented before (see e.g. Pye et al. 1994, Hodgkin et al. 1995, Neuhäuser 1997) and some of the flares discussed here have been discussed by Gagné et al. (1995), Strom & Strom (1994), and Preibisch et al. (1993). However, this is the first statistical evaluation of flare luminosities. Flare rates comparing stellar subgroups with different properties (such as age,  $v \sin i$ , and stellar multiplicity) are compiled in Sect. 7. Because of lack of sufficient statistics for a detailed spectral analysis, hardness ratios are used to describe the spectral properties of the flares. In Sect. 8 we present the observed relations between hardness ratios measured during different activity phases and between hardness and X-ray luminosity. Finally, we discuss and summarize our results in Sect. 9 and Sect. 10.

## 2. Database and data reduction

In this section we introduce the stellar sample and explain the analysis of the raw data. Details about our membership lists for TTSs, Pleiads, and Hyads are given below (Sect. 2.1). We have retrieved all pointed *ROSAT* PSPC observations from the archive that contain at least one of the stars from these lists in their field. The observations are listed in Table 1. After performing source detection on all of these pointings, we have cross correlated the membership lists with the detected X-ray sources and identified individual TTSs, Pleiads, and Hyads in the X-ray image. The process of source detection and identification is described in Sect. 2.2.

### 2.1. The stellar sample

The analysis presented here is confined to the Taurus-Auriga-Perseus region. This portion of the sky includes the Taurus-Auriga complex, the MBM 12 cloud, and the Perseus molecular clouds with the reflection nebula NGC 1333 and the young cluster IC 348. Two open clusters containing mostly ZAMS stars are found nearby the above mentioned star forming regions, the Pleiades and the Hyades. The choice of this specific sky region thus enables us to compare the X-ray emission of young stars at different ages.

Our sample of low-mass PMS stars in and around Taurus consists of all TTSs which are either on or very close to the Taurus star forming clouds or off the clouds at locations where they can still be linked with the Taurus clouds (see e.g. Neuhäuser et al. 1997). We restrict our Taurus sample to objects between  $\alpha_{2000} = 2h$  and  $5h$  and  $\delta_{2000} = -10^\circ$  and  $40^\circ$ . The TTSs in Taurus comprise those listed in the Herbig-Bell catalog (Herbig & Bell 1988; HBC), in Neuhäuser et al. (1995) or in Kenyon & Hartmann (1995). In addition we include TTSs newly identified either as counterparts to previously unidentified *ROSAT* sources (Strom & Strom 1994, Wichmann et al. 1996, Magazzù et al. 1997, Neuhäuser et al. 1997, Zickgraf et al. 1998,

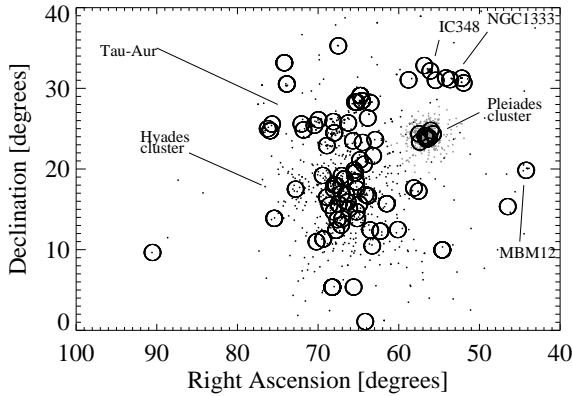


**Fig. 1.** Sky map of the Tau-Aur-Per region showing the pointing positions of the *ROSAT* PSPC observations. On display are all PSPC pointings selected from the *ROSAT* Public Data Archive which contain at least one TTS, Pleiad, or Hyad from the membership lists given in the text. In addition all stars from the membership lists are plotted.

Li & Hu 1998, Briceño et al. 1998) or by other means (Torres et al. 1995, Oppenheimer et al. 1997, Briceño et al. 1998, Reid & Hawley 1999, Gizis & Reid 1999). TTSs in the molecular cloud MBM 12 (see Hearty et al. 2000) are also in the examined sky region.

In addition to TTSs from Tau-Aur we include those from the Perseus molecular cloud complex, mainly IC 348 and NGC 1333, in our analysis. Our list of TTSs in IC 348 comprises X-ray detections identified with  $H\alpha$  emission stars or with proper motion members (Tables 4 and 5 in Preibisch et al. 1996), and emission line stars from Herbig (1998), and Luhman (1999). TTS members of NGC 1333 are listed in Preibisch (1997).

All objects with low lithium strength are excluded, because it is dubious whether they are young. We accept only those objects as PMS stars which show more lithium than Pleiades stars of the same spectral type, i.e. we exclude all those with  $W_\lambda(\text{Li})$  lower than  $0.2 \text{ \AA}$  for F- and G-type stars and lower than  $0.3 \text{ \AA}$  for K-type stars. When applying this criterion, we always use the spectrum with the best resolution and best S/N, i.e. the high-resolution spectra from Wichmann et al. (in preparation). If no high-resolution spectra are available, we use the medium-resolution spectra from Martín & Magazzù (1999), Neuhäuser et al. (1997), or Magazzù et al. (1997).

Members of the Pleiades and Hyades clusters are selected from the Open Cluster database compiled by C. Prosser and colleagues (available at <http://cfa-www.harvard.edu/~stauffer/openc1/index.html>). The tables collected in Prosser's database provide a summary of membership classification based on different methods, such as photometry, spectra, radial velocity and  $H\alpha$  emission. In addition a final membership determination is given which we use to define our membership lists.

Fig. 1 shows a sky map with the positions of the selected PSPC observations.

## 2.2. Source detection and identification

Source detection is performed on all observations given in Table 1 and shown in Fig. 1 using a combined local and map source detection algorithm based on a maximum likelihood method (Crudace et al. 1988). All detections with  $ML \geq 7.4$  (corresponding to  $\sim 3.5$  Gaussian  $\sigma$  determined as best choice by Neuhäuser et al. 1995) are written to a source list, which is subsequently cross-correlated with the membership lists introduced above. The maximum distance  $\Delta$  between optical and X-ray position to be allowed in this identification process depends on the off-axis angle of the source because the positional accuracy of the PSPC is worse at larger distances from the center due to broader point spread function (PSF). From distributions of the normalized cumulative number of identifications versus offset  $\Delta$  for different off-axis ranges we have determined the optimum cross-correlation radius for all detector positions (similar to Neuhäuser et al. 1995). A detailed description of this process together with a table providing  $\Delta$  for different off-axis ranges will be given in Stelzer et al. (in preparation).

Observations which are characterized by strong background variations (200020, 200008-0, and 200442), as well as observations consisting of two very short intervals separated by a gap of  $> 100 \text{ h}$  (200068-0, 200914) are omitted from the flare detection and flare analysis. Furthermore, we neglect observations with a total duration of less than 1000 s. All observations which have been ignored in the analysis presented in this paper are marked with an asterisk in Table 1.

## 3. Lightcurves

Using the arrival time information of the photons counted within a pre-defined source circle lightcurves are generated for each of the *ROSAT* sources that have been identified with a TTS, Pleiad or Hyad from the membership lists.

For the source extraction radius we have used the 99% quantile of the Point Spread Function (PSF) at 1 keV, i.e. the radius containing 99% of the 1 keV photons at the respective off-axis angle. In contrast to the standard EXSAS source radius of 2.5 FWHM, which becomes unreasonably large for off-axis sources due to the extended wings of the PSF, this choice of extraction radius limits the source size. Close to the detector center, some bright sources slightly overshine the nominal 99% quantile of the PSF probably due to small deviations from the assumed 1 keV spectrum. We have therefore checked all images for such bright sources and determined a larger source radius for these cases based on visual inspection. In crowded regions, where the PSF of several sources overlap, the measured counts are upper limits to the actual emission of the sources. None of the overlapping sources showed a flare, however, such that no further attention is drawn to the overestimation of the count rate in these cases.

**Table 1.** Complete list of *ROSAT* PSPC pointings available from the *ROSAT* Public Data Archive in October 1998, which include at least one TTS, Pleiad or Hyad from our membership lists (see text) in the field of view. All observations *not* marked by an asterisk have been analyzed in this work. The total exposure time is given in Column 3. The remaining columns give the number of detected and undetected TTSs, Pleiads and Hyads (D – detection, N – non-detection). If more than one star was identified with an X-ray source all identifications are listed. For multiple systems each component is counted as one entry.

No.	<i>ROSAT</i> Pointing ID	exp (s)	TTS		Pleiads		Hyads	
			D/	N	D/	N	D/	N
1	180185p	8897	16/	7	0/	0	0/	0
2	200001p-1	1520	0/	2	0/	0	0/	0
3	200001p-0	4486	23/	12	0/	0	0/	0
4	200001p-1	25591	26/	9	0/	0	0/	0
5	200008p-2*	696	0/	6	2/	162	0/	0
6	200008p-4*	121	0/	5	0/	220	0/	0
7	200008p-5*	722	0/	4	1/	110	0/	2
8	200008p-0*	5936	2/	4	86/	165	1/	0
9	200008p-2	7049	4/	3	88/	161	1/	0
10	200020p*	39879	0/	2	0/	0	13/	8
11	200068p-1	1307	3/	2	49/	184	0/	0
12	200068p-0*	12849	3/	2	93/	155	1/	0
13	200068p-1	27071	3/	2	101/	145	1/	0
14	200073p	2376	0/	1	0/	0	6/	3
15	200082p-1*	814	0/	0	0/	0	0/	2
16	200083p	2799	0/	0	0/	0	16/	5
17	200107p-1	27692	0/	0	0/	0	2/	1
18	200107p-0	3923	0/	0	0/	0	2/	1
19	200402p	10469	3/	0	0/	0	0/	0
20	200441p	10987	0/	3	0/	0	15/	8
21	200442p	19948	2/	0	0/	0	6/	4
22	200443p	20074	15/	8	0/	0	12/	2
23	200444p	14593	0/	1	0/	0	2/	5
24	200547p	28359	0/	3	0/	0	0/	0
25	200553p	10961	0/	0	0/	0	8/	3
26	200556p	22456	5/	0	67/	81	3/	0
27	200557p	27648	7/	0	94/	96	0/	0
28	200576p	1521	0/	0	0/	0	12/	2
29	200677p*	650	3/	13	0/	0	3/	0
30	200694p	1987	17/	13	0/	0	1/	1
31	200694p-1	5395	16/	12	0/	0	2/	0
32	200775p	4096	0/	2	0/	0	3/	9
33	200776p	22995	0/	1	0/	0	10/	5
34	200777p	16296	0/	1	0/	0	13/	8
35	200778p	1900	0/	1	0/	0	15/	11
36	200911p	17460	0/	0	0/	0	7/	4
37	200911p-1	13755	0/	0	0/	0	7/	4
38	200912p	1656	0/	2	0/	0	3/	6
39	200912p-1	23710	1/	1	0/	0	5/	4
40	200913p	25341	2/	0	0/	0	7/	2
41	200914p*	4098	0/	0	0/	0	1/	1
42	200915p	3504	0/	0	0/	0	2/	2
43	200942p	7367	0/	0	0/	0	4/	6
44	200945p	4099	0/	0	0/	0	7/	4
45	200949p	6098	17/	3	0/	0	0/	0
46	200980p	10649	0/	0	0/	0	3/	3
47	200980p-1	4014	0/	0	0/	0	3/	3
48	200981p	4491	2/	1	0/	0	8/	7
49	200982p	7724	0/	0	0/	0	10/	3
50	201012p	7492	2/	1	0/	0	0/	0
51	201013p	4826	3/	2	0/	0	0/	0
52	201013p-1	4484	2/	4	0/	0	0/	0
53	201014p	9910	1/	1	0/	0	1/	1
54	201015p	10058	0/	1	0/	0	1/	1
55	201016p	10576	6/	6	0/	0	0/	0
56	201017p	8452	7/	9	0/	0	0/	0
57	201023p	3058	0/	0	0/	0	0/	3
58	201025p	5448	11/	17	0/	0	0/	0
59	201097p	10287	0/	0	0/	0	1/	0
60	201278p	1358	4/	0	0/	0	0/	0
61	201278p-1	4028	4/	0	0/	0	0/	0
62	201305p	23643	94/	96	0/	0	0/	0
63	201312p	2800	8/	26	0/	0	0/	0
64	201313p	4027	22/	12	0/	0	7/	6
65	201314p	2691	0/	0	0/	0	12/	4
66	201314p-1	1397	0/	0	0/	0	9/	6

**Table 1. continued**

No.	<i>ROSAT</i> Pointing ID	exp (s)	T		P		H	
			D/	N	D/	N	D/	N
67	201315p*	645	4/	1	0/	0	1/	9
68	201315p-1	1544	5/	0	0/	0	4/	7
69	201315p-2	2298	5/	0	0/	0	4/	6
70	201316p	4156	1/	1	0/	0	3/	3
71	201317p	1731	0/	0	0/	0	1/	1
72	201319p	1811	4/	0	0/	0	3/	1
73	201368p	16594	0/	1	0/	0	17/	9
74	201369p	15538	0/	0	0/	0	24/	4
75	201370p	4975	0/	1	0/	0	5/	4
76	201370p-1	13652	1/	0	0/	0	5/	2
77	201484p	7673	1/	0	0/	0	0/	0
78	201485p	2429	0/	3	0/	0	0/	0
79	201485p-1	1904	1/	2	0/	0	0/	0
80	201504p	109534	2/	0	0/	0	4/	0
81	201519p	5889	2/	0	0/	0	0/	0
82	201532p	10183	9/	6	0/	0	1/	0
83	201533p	10799	4/	6	0/	0	0/	0
84	201534p	6213	0/	1	0/	0	3/	1
85	201598p	5652	7/	14	0/	0	0/	0
86	201599p	6175	6/	15	0/	0	0/	0
87	201600p	5747	6/	15	0/	0	0/	0
88	201601p	5817	5/	16	0/	0	0/	0
89	201602p	5582	8/	13	0/	0	0/	0
90	201747p	19600	0/	1	0/	0	16/	2
91	201748p	16999	0/	0	0/	0	2/	3
92	201749p*	924	0/	0	0/	0	3/	1
93	201749p-1	1540	0/	0	0/	0	3/	1
94	300178p	710	0/	7	0/	0	0/	0
95	400312p	10735	0/	0	0/	0	1/	0
96	700044p	4611	5/	0	0/	0	6/	4
97	700063p	1701	0/	0	0/	0	1/	0
98	700825p	1435	0/	0	0/	0	0/	2
99	700825p-1	15744	0/	0	0/	0	1/	1
100	700913p	2096	0/	0	0/	0	1/	0
101	700916p	7161	0/	0	0/	0	1/	0
102	700919p	2004	0/	0	0/	0	1/	0
103	700945p	2516	0/	0	0/	0	1/	0
104	701055p	9039	0/	0	0/	0	0/	0
105	701253p	5417	0/	0	0/	0	0/	2
106	800051p-0	1470	1/	0	0/	0	0/	0
107	800051p-1	3347	1/	0	0/	0	0/	0
108	800051p-2	3303	1/	0	0/	0	0/	0
109	800083p	10220	1/	0	0/	0	0/	0
110	800104p	7524	1/	0	0/	0	0/	0
111	800193p	21969	0/	0	0/	0	3/	3
112	900138p	24899	6/	0	0/	0	0/	0
113	900154p	28791	0/	2	0/	0	0/	0
114	900193p	9128	3/	22	0/	0	0/	0
115	900353p	7718	18/	11	0/	0	12/	4
116	900371p	4227	1/	0	0/	0	2/	0
117	900371p-1	7718	0/	0	0/	0	2/	0

The events measured within the circular source region are binned into 400 s intervals. Since the typical duration of a flare is less than one hour, significantly longer integration times would lead to a loss of information about the structure of the lightcurve, while for shorter bin lengths the lightcurves are dominated by the low statistics. Furthermore, the choice of 400 s integration time guarantees that no additional variability is introduced by the telescope motion (wobble).

Due to the earth eclipses the data stream is interrupted at periodical time intervals. Depending on the phase used for the time integration, at the beginning and/or end of each data segment the 400 s intervals are only partly exposed. For the flare detection only bins with full 400 s of exposure are used. To gain independence of the binning we generate lightcurves with different phasing of the 400 s intervals: First, in order to divide the given observing time into as many 400 s exposures as possible,

a lightcurve is binned in such a way that a new 400 s interval starts after each observation gap. Thus, data are lost only at the end of each data segment, because the last bin remains uncomplete. Secondly, lightcurves are built by simply splitting the total observing time into 400 s intervals beginning from the start of the observation regardless of data gaps. In this case data are rejected at the beginning *and* end of each data segment.

The number of background counts falling in the source circle is determined from the smoothed background image which is created by cutting out the detected sources and then performing a spline fit to the resulting image. This method of background acquisition is of advantage in crowded fields where an annulus around the source position – the most widely used method for estimating the background – likely is contaminated by other sources. The background count rate is found by dividing the number of background counts in the source circle through the exposure time extracted from the standard *ROSAT* exposure map. To take account of possible time variations in the background count rate, the background is determined separately for each data segment and subtracted from the measured count rate in the respective data interval. (When referring to ‘data segments’ we mean parts of the lightcurve that are separated from each other by gaps of at least 0.5 h.)

## 4. Flare detection

### 4.1. The method

One of the major elements of a flare by customary definition is a significant increase in count rate, after which the initial level of intensity is reached again. Therefore, our flare detection is based on the deviation of the count rate from the (previously determined) mean quiescent level of the source. To ensure that the quiescent count rate contains no contribution from flares, in the first step, we determine mean count rates for all data segments of each lightcurve and define the quiescent level as the lowest mean measured in any of these data segments.

We define a flare as an event which is characterized by two or more consecutive time bins that constitute a sequence of either rising or falling count rates, corresponding to rise and decay phase of the flare. In addition, to ensure the significance of our flare detections, we define the upper standard deviation of the quiescent level as a point of reference and require that (a) all bins which are part of the flare are characterized by count rates higher than this level, and that (b) the sum of the deviations of all these bins is more than  $5\sigma$  from this level. A rise immediately followed by a decay is counted as *one* flare. Since the shape of a lightcurve is influenced to some degree by the binning used, we accept only flares that are detected in lightcurves with both bin phasings (see Sect. 3).

Detections of more than one flare in a single lightcurve are possible. To estimate the contribution of each event properly, after detection the decay of the first flare in each lightcurve is modeled by an exponential function, and a new lightcurve is generated by subtracting the fit function from the data. Having removed the first flare, we search for further flares in the reduced, ‘flare-subtracted’ lightcurve using the same criteria as

before. This procedure is repeated until no additional flares are detected.

Since many of the investigated sources are highly variable X-ray emitters on timescales shorter than resolvable by our method, the mean count rate used until now in some cases is not a good estimate for the quiescent emission. With the knowledge obtained about the times at which flares have occurred we therefore redetermine the quiescent count rate taking the mean from the remaining data after removal of all flare contributions. Using this new mean count rate we repeat the flare detection procedure.

### 4.2. Flare Parameters

With the detection procedure described in the previous subsection we have found 52 flares. We have always identified the nearest optical position with the X-ray source. In one flare, however, two possible optical counterparts, DD Tau and CZ Tau, are closeby (at  $6''$  and  $24''$  respectively), so that we can not be sure which star flared. Fifteen events were observed on TTSSs, 20 on Pleiads, and 17 on Hyads. On two TTSSs (RXJ 0437.5+1851 and T Tau) and two Hyads (VA 334 and VB 141) two flares occurred in the same observation. VB 141 showed a third event during a different *ROSAT* exposure.

Hyades stars above  $2 M_{\odot}$ , that have already evolved off the main-sequence, are not considered in the statistical analysis if they showed a flare. Brown dwarfs in the Hyades and Pleiades are not on the main-sequence per definition, but they are also too faint for X-ray detection (Neuhäuser et al. 1999). Thus we discuss only the ZAMS from the Pleiades and Hyades.

A complete list of all TTSSs, Pleiads, and Hyads on which at least one flare was detected is given in Table 2. Column 1 gives the designation of the flaring star. Column 2 is the distance estimate used for the count-to-energy-conversion. For TTSSs in Taurus-Auriga we adopt a value of 140 pc (Elias 1978, Wichmann et al. 1998), while the TTSSs in MBM 12 are located at 65 pc (Hearty et al. 2000), and those in Perseus are located at 350 pc (NGC 1333; Herbig & Bell 1988) and 300 pc (IC 348; Cernicharo et al. 1985). Pleiads are assumed to be at a distance of 116 pc, the value derived by Mermilliod et al. (1997). Finally, we use the individual Hipparcos parallaxes for Hyades stars if available, and otherwise the mean value of 46 pc (Perryman et al. 1998). We give spectral type,  $v \sin i$ , multiplicity, and binary separation of the stars and their respective references in columns 3 – 9. For TTSSs additional columns specify whether the star is a cTTS or a wTTS.

The lightcurves of all flares have been analyzed by fitting an exponential to the decay of each flare. In Figs. 2, 3, and 4 the fit function and measured mean quiescent count rate are displayed together with the data. In Tables 3, 4 and 5 we give the result of the modeling. Column 1 and column 2 contain the stellar identification of the X-ray source and the *ROSAT* observation request number (ROR). The mean quiescent count rate is given in column 3, the maximum count rate inferred from the exponential fit to the lightcurve in column 4, and the decay timescale  $\tau_{\text{dec}}$  from the fit in column 5. For flares with poor

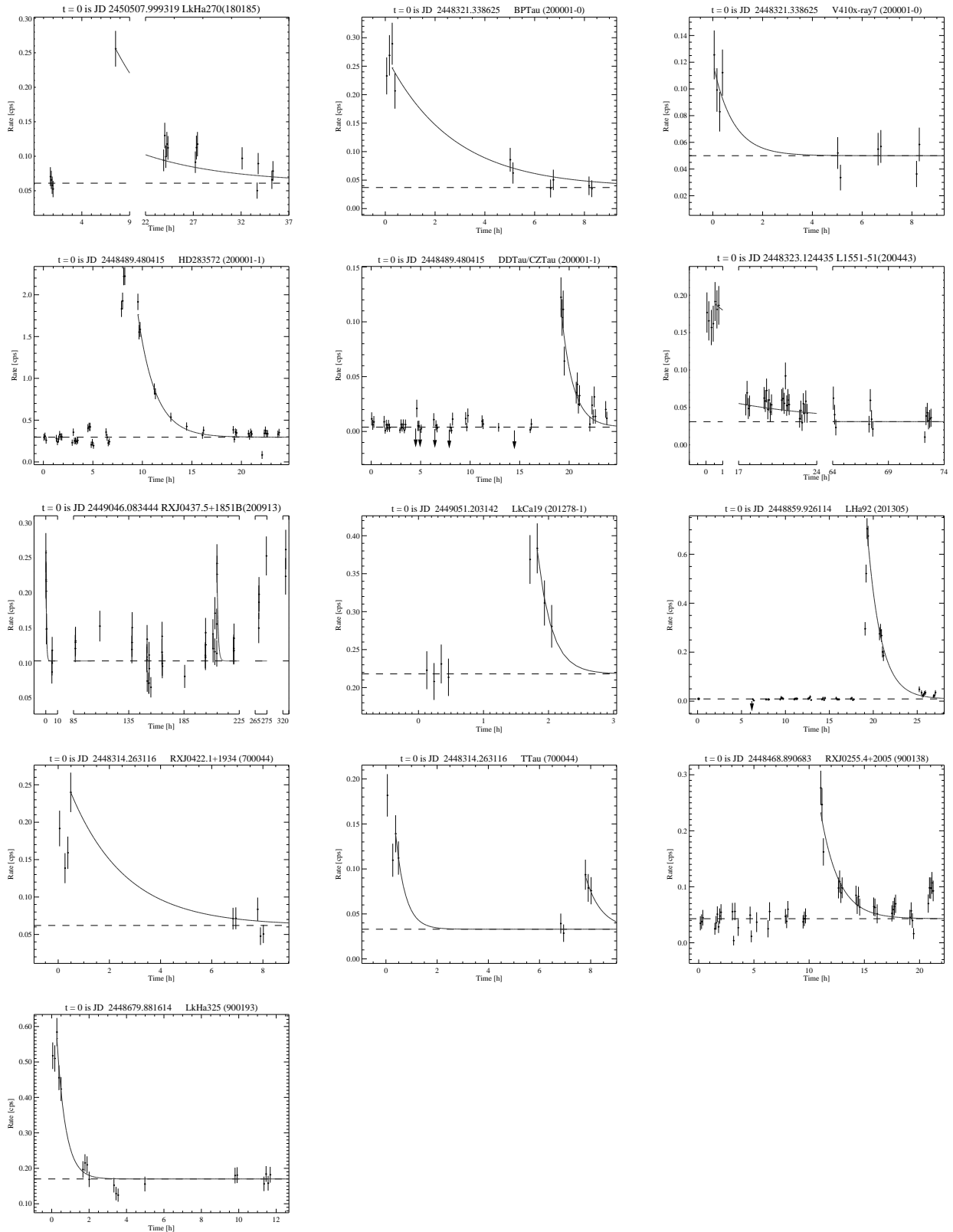


**Fig. 2.** PSPC lightcurves for flares on TTSs in Taurus-Auriga and Perseus detected by the procedure described in Sect. 4.1. Identification of the X-ray source and *ROSAT* observation request number (in brackets) are given for each source. Binsize is 400 s,  $1\sigma$  uncertainties. The dashed line represents the quiescent count rate. Solid lines are exponential fits to the data points belonging to the flare down to the quiescent emission. Background count rates are shown as upper limits when the background subtracted count rate is below zero.

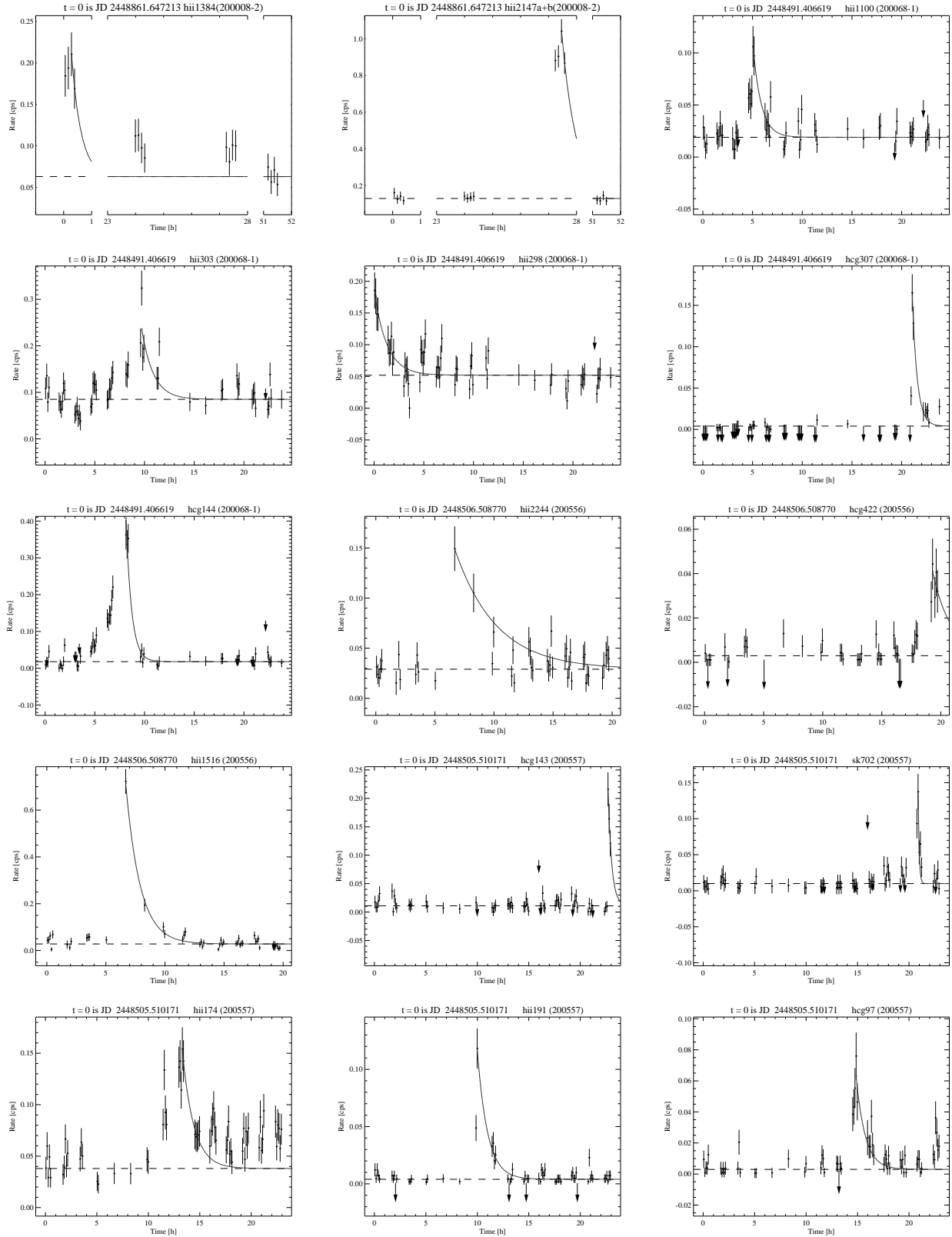


**Fig. 3.** PSPC lightcurves for flares on members of the Pleiades cluster detected by the procedure described in Sect 4.1. Identification of the X-ray source and *ROSAT* observation request number (in brackets) are given for each source. Binsize is 400 s,  $1\sigma$  uncertainties. The dashed line represents the quiescent count rate. Solid lines are exponential fits to the data points belonging to the flare down to the quiescent emission. Background count rates are shown as upper limits when the background subtracted count rate is below zero.

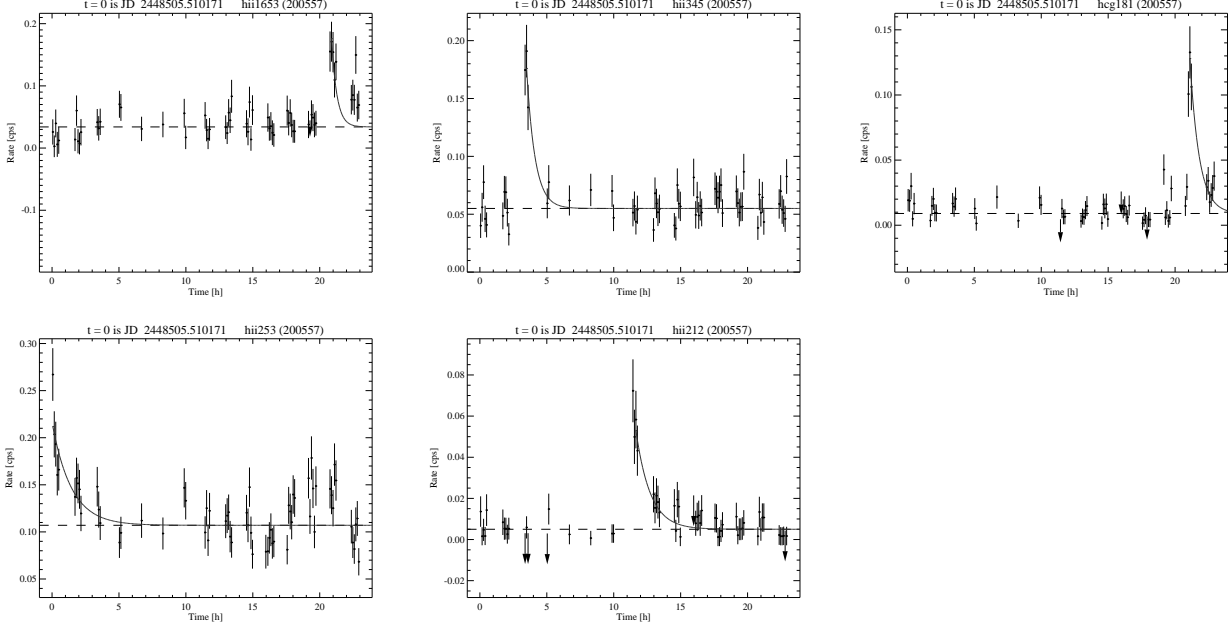


**Fig. 3.** *continued*

data sampling we did not determine the errors of  $\tau_{\text{dec}}$ . Column 6 is the estimated rise time of the flare. Due to data gaps in most cases no reasonable estimate can be given. Luminosities are listed in columns 7 and 8: quiescent luminosity  $L_{\text{qui}}$ , and maximum luminosity during the flare  $L_{\text{max}}$ . We assume that all stars in the system contribute the same level of X-ray emission during quiescence, but that only one component flares at any one time. Therefore, for all multiple stars the observed quiescent count rate from column 3 has been divided by the number of components before the conversion to luminosity and energy.

For the conversion from count rates to luminosities we have used the mean *ROSAT* PSPC energy-conversion-factor (ECF) from Neuhäuser et al. (1995), i.e.  $ECF = 1.1 \cdot 10^{11}$  cts cm<sup>2</sup>/erg and the distances given in Table 2. In order to eliminate uncertainties in the distance estimate we have computed ratios of luminosity (given in column 9). Here,  $L_F$  denotes the luminosity emitted during the flare, i.e.  $L_F = L_{\text{max}} - L_{\text{qui}}$ . The total emitted energy during quiescence  $E_{\text{qui}}$  (column 10) and during the flare alone  $E_F$  (column 11) are inferred from the integration of the lightcurve between  $t_{\text{max}}$  and  $t_{\text{max}} + \tau$ . The last column gives the reference for flares that have been published previously. In the last two rows of Tables 3, 4 and 5 we have listed the mean and median for each of the given parameters, except  $\tau_{\text{ris}}$  which is not well constrained. The means and medians have been computed with the ASURV Kaplan-Meier estimator (see Feigelson & Nelson 1985), taking account of upper/lower limits. Lower limits of  $L_{\text{max}}$  occur when there is doubt about whether the maximum emission of the flare has been observed (due to a data gap near the observed maximum). Upper limits for  $\tau_{\text{dec}}$  occur when the decay is not observed because of a data gap between maximum

and post-flare quiescent count rate. Both luminosity and decay timescale determine the flare energy, but the limits of these two parameters carry opposite signs. We therefore consider all values of  $E_F$  uncertain where  $\tau_{\text{dec}}$  or  $L_{\text{max}}$  are a limit (indicated by colons in Tables 3, 4 and 5) and have not included them in the computation of the mean and median.

## 5. Observational selection effects

It is the purpose of this paper to compare the flare activity of different stars, and thus some attention has to be drawn to observational selection effects. In this section, we will discuss how observational restrictions influence the search for flares. At several points during the data analysis, we are confronted with the problem of finding a representation of the data which is free from these biases.

The major difficulty with the statistical evaluation of flares on different stars is that the sensitivity of the flare detection process depends on the measured (quiescent) count rate, which determines the signal-to-noise (S/N), and hence on the distance to the star. The observational bias consists in the fact that for bright stars ( $L_{\text{qui}}$  large) the minimum luminosity  $L_F$  of a detectable flare is higher than for a faint star. The result is, among others, that at first hand it can not be decided whether any observed correlation between  $L_{\text{qui}}$  and  $L_F$  is real or produced by this effect. In Fig. 5 we have plotted the flare luminosity  $L_F$  against the quiescent luminosity  $L_{\text{qui}}$ .

The contribution of the observational bias to this correlation can be estimated as follows: For each quiescent count rate  $I_{\text{qui}}$  we can determine the minimum strength  $L_F/L_{\text{qui}}$  needed for a flare to be detected, if we assume that a flare is found whenever there is a rise in count rate of at least  $3\sigma$  within one 400 s



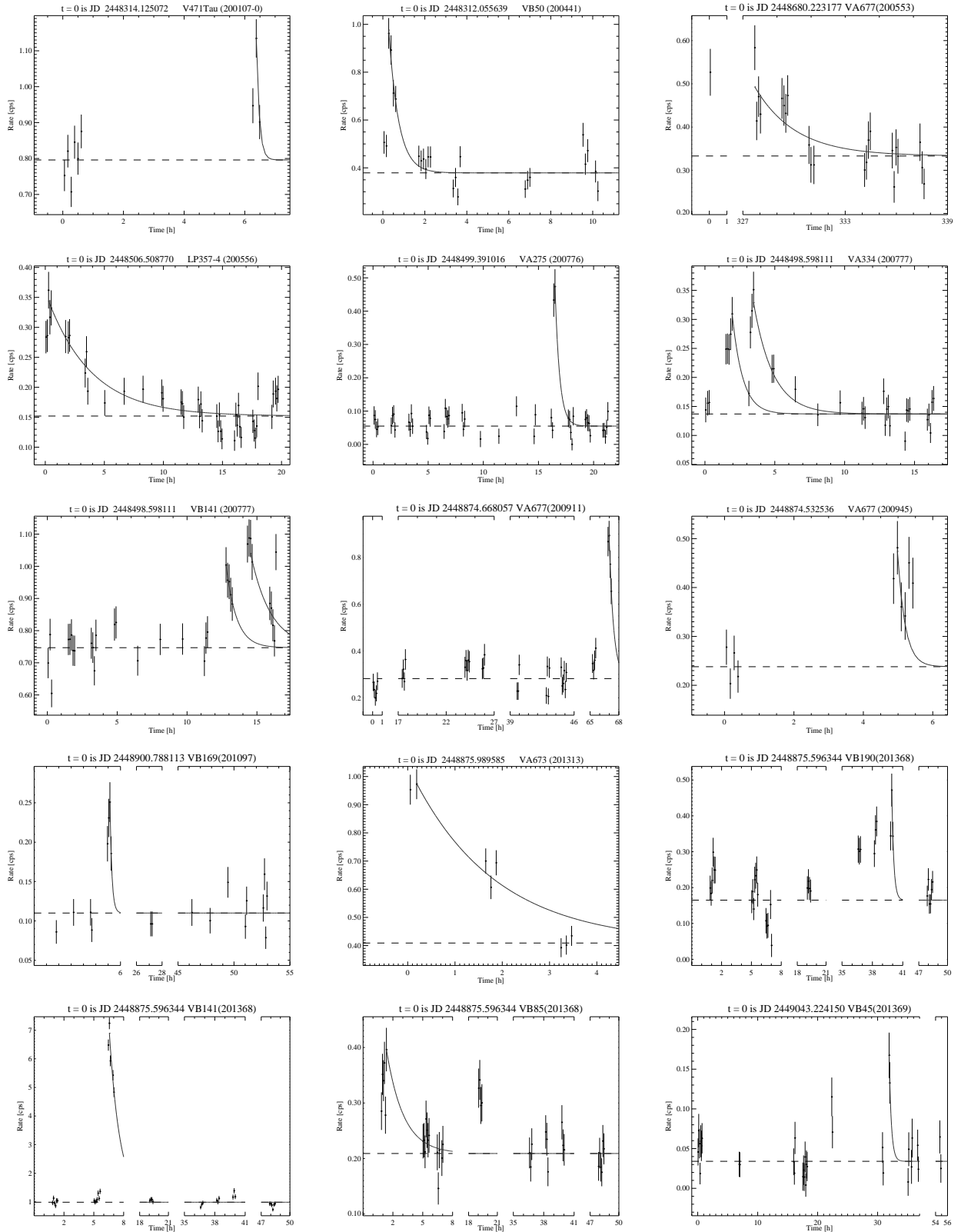


**Fig. 4.** PSPC lightcurves for flares on members of the Hyades cluster detected by the procedure described in Sect 4.1. Identification of the X-ray source and *ROSAT* observation request number (in brackets) are given for each source. Binsize is 400 s,  $1\sigma$  uncertainties. The dashed line represents the quiescent count rate. Solid lines are exponential fits to the data points belonging to the flare down to the quiescent emission. Background count rates are shown as upper limits when the background subtracted count rate is below zero.

**Table 2.** Properties of stars in Tau-Aur-Per which flared during at least one *ROSAT* PSPC observation. Spectral types marked with an asterisk are determined from  $B - V$  or  $R - I$  given in the Open Cluster database using the conversion given by Schmidt-Kaler (1982). The meaning of the flags in column ‘Multiplicity’ is: B for binary, SB1 for single-lined spectroscopic binary, and SB2 for double-lined spectroscopic binary. For one flare on TTSs it is not clear whether it belongs to DD Tau, a cTTS, or CZ Tau, a wTTS, because the spatial resolution of the PSPC is too low to resolve these stars. DD Tau and CZ Tau both are binaries. Only flares on stars of spectral type G and later are analysed in the remainder of this paper.

Designation	Distance [pc]	Sp.Type (Ref)	vsini (Ref) [km/s]	Mult	Binary sep [ $''$ ]	TTS Type
<b>T Tauri Stars</b>						
LkH $\alpha$ 270	350.0	K7M0	(1)			C (1)
BPTau	140.0	K7	(1)	10.0 (17)		C (1)
V410x-ray7	140.0	M1	(2)			W (2)
HD283572	140.0	G5 I	(1)	75.6 (18)		W (1)
DDTau/CZTau	140.0	M1/M1.5	(1)		B/B 0.57/0.33 (27)	C/W (1)
L1551-51	140.0	K7	(1)	27.0 (1)		W (1)
RXJ0437.5+1851 B	140.0	M0.5	(3)	10.5 (3)	B 4.30 (28)	W (3)
LkCa19	140.0	K0	(1)	18.6 (17)		W (1)
LH $\alpha$ 92	300.0	K0	(5)			C (1)
RXJ0422.1+1934	140.0	M4.5	(4)		B 12.0 (28)	C (4)
TTau	140.0	K0	(1)	20.7 (17)	B 0.71 (29)	C (1)
RXJ0255.4+2005	65.0	K6	(6)	10.0 (6)		W (6)
LkH $\alpha$ 325	350.0	K7M0	(1)		B 11.0 (30)	W (1)
<b>Pleiads</b>						
hii1384	116.0	A4V	(7)	215.0 (19)		-
hii2147	116.0	G9	(8)	6.9 (20)	SB2 (31)	-
hii1100	116.0	K3	(8)	5.4 (20)	B 0.78 (32)	-
hii303	116.0	K1.4*	(9)	17.4 (20)	B 1.81 (32)	-
hii298	116.0	K1.4*	(9)	6.6 (20)	B 5.69 (32)	-
hcg307	116.0			13.0 (21)		-
hcg144	116.0					-
hii2244	116.0	K2.5	(10)	50.0 (22)		-
hcg422	116.0					-
hii1516	116.0	K7*	(11)	105.0 (20)		-
hcg143	116.0	M2*	(11)			-
sk702	116.0					-
hii174	116.0	K0.8*	(9)	28.0 (23)		-
hii191	116.0	K7.7	(12)	9.1 (20)		-
hcg97	116.0					-
hii1653	116.0	K6	(8)	21.0 (8)		-
hii345	116.0	G8	(10)	18.9 (20)		-
hcg181	116.0	M1.5*	(11)			-
hii253	116.0	G1	(10)	37.0 (23)		-
hii212	116.0	M0.0	(12)	10.0 (8)		-
<b>Hyads</b>						
V471Tau	46.8	K1.2*	(13)			-
VB50	44.9	G1V	(14)		SB? (33)	-
VA677	57.0	K	(15)	24.0 (24)	SB2 (24)	-
LP357-4	46.3	M3	(15)			-
VA275	46.3	M2-3	(15)	10.0 (25)		-
VB141	47.9	A8*	(16)			-
VA334	41.0	M0	(15)	6.0 (24)		-
VB169	46.5	A6.6*	(16)			-
VA673	46.3	M1	(15)		SB (34)	-
VB190	46.3	K	(15)	8.5 (24)	SB (32)	-
VB85	41.2	F5V	(14)	55.0 (26)		(35) -
VB45	47.2	Am	(14)	12.0 (26)	SB1 (26)	-

**Catalogues:** VB - van Bueren 1952, VA - van Altena 1969, LP - Luyten et al. 1981, hii - Hertzsprung 1947, hcg - Haro et al. 1982, sk - Stauffer et al. 1991

**References:** (1) - Herbig & Bell 1988, (2) - Strom & Strom 1994, (3) - Wichmann et al. (in preparation), (4) - Martín & Magazzù 1999, (5) - Herbig 1998, (6) - Hearty et al. 2000, (7) - Mendoza 1956, (8) - Stauffer & Hartmann 1987, (9) - Johnson & Mitchell 1958, (10) - Soderblom et al. 1993a, (11) - Stauffer 1982, Stauffer 1984, (12) - Prosser et al. 1991, (13) - priv. comm. between J. Stauffer and E. Weis according to the Open Cluster data base, (14) - Morgan & Hiltner 1965, (15) - Pesch 1968, (16) - Morel & Magnenat 1978, (17) - Hartmann & Stauffer 1989, (18) - Walter et al. 1987, (19) - Anderson et al. 1966, (20) - Quelez et al. 1998, (21) - Jones et al. 1996, (22) - Stauffer et al. 1984, (23)

**Table 3.** Parameters derived from the lightcurves of flares on T Tauri Stars detected in the *ROSAT* PSPC observations from Table 1 (see Sect. 4.2 for an explanation). The last column gives the reference for flares that have been presented elsewhere in the literature: [a] Strom & Strom (1994), [b] Preibisch et al. (1993), but newly reduced here. In the last two rows we give the mean (determined by taking account of lower/upper limits) and the median for each parameter.

Desig.	ROR	$I_{\text{qui}}$ [cps]	$I_{\text{max}}$ [cps]	$\tau_{\text{dec}}$ [h]	$\tau_{\text{ris}}$ [h]	$L_{\text{qui}}$ [erg/s]	$L_{\text{max}}$ [erg/s]	$L_{\text{F}}/L_{\text{qui}}$	$E_{\text{qui}}$ [erg]	$E_{\text{F}}$ [erg]	Notes
LkH $\alpha$ 270	180185	$0.061 \pm 0.008$	$0.256 \pm 0.008$	<8.85	< 7.84	8.13e+30	> 3.41e+31	> 3.197	2.59e+35	5.23e+35:	
BPTau	200001-0	$0.037 \pm 0.004$	$0.247 \pm 0.034$	2.67 <sup>+0.96</sup> <sub>-0.92</sub>	> 0.22	7.89e+29	5.27e+30	5.676 $\pm$ 1.110	7.58e+33	2.73e+34	
V410x-ray7	200001-0	$0.050 \pm 0.011$	$0.114 \pm 0.018$	0.80 <sup>+7.22</sup> <sub>-0.53</sub>	> 0.00	1.07e+30	> 2.43e+30	> 1.280	3.07e+33	> 2.52e+33:	
HD283572	200001-1	$0.296 \pm 0.069$	$1.762 \pm 0.101$	1.78 <sup>+0.18</sup> <sub>-0.19</sub>	< 1.56	6.31e+30	3.76e+31	4.953 $\pm$ 1.226	4.04e+34	1.27e+35	[a]
DDTau/CZTau	200001-1	$0.004 \pm 0.005$	$0.113 \pm 0.013$	1.19 <sup>+0.28</sup> <sub>-0.27</sub>	< 2.99	2.13e+28	> 2.41e+30	>112.000	9.14e+31	> 6.24e+33:	[a]
L1551-51	200443	$0.031 \pm 0.015$	$0.188 \pm 0.027$	<8.83	> 0.48	6.61e+29	4.01e+30	5.065 $\pm$ 2.645	2.10e+34	> 6.74e+34:	
RXJ0437.5+1851	200913	$0.103 \pm 0.027$	$0.259 \pm 0.037$	0.49 <sup>+0.27</sup> <sub>-0.18</sub>	> 0.00	1.10e+30	5.52e+30	4.029 $\pm$ 1.304	1.94e+33	3.75e+33	
RXJ0437.5+1851	200913	$0.103 \pm 0.027$	$0.242 \pm 0.027$	0.94	> 0.11	1.10e+30	5.16e+30	3.699 $\pm$ 1.133	3.72e+33	6.35e+33	
LkCa19	201278-1	$0.218 \pm 0.010$	$0.382 \pm 0.040$	0.22 <sup>+0.22</sup> <sub>-0.09</sub>	< 1.36	4.65e+30	8.15e+30	0.752 $\pm$ 0.192	3.68e+33	1.72e+33	
LH $\alpha$ 92	201305	$0.009 \pm 0.009$	$0.699 \pm 0.029$	1.55 <sup>+0.11</sup> <sub>-0.12</sub>	< 1.50	8.81e+29	6.84e+31	76.667 $\pm$ 76.741	4.92e+33	2.38e+35	[b]
RXJ0422.1+1934	700044	$0.062 \pm 0.016$	$0.240 \pm 0.016$	<2.15	> 0.43	6.61e+29	> 5.12e+30	> 6.742	5.12e+33	1.86e+34:	
TTau	700044	$0.033 \pm 0.008$	$0.139 \pm 0.008$	0.38	> 0.00	3.52e+29	> 2.96e+30	> 7.424	4.81e+32	> 1.94e+33:	
TTau	700044	$0.033 \pm 0.008$	$0.092 \pm 0.018$	0.61 <sup>+5.46</sup> <sub>-0.41</sub>	> 0.85	3.52e+29	> 1.96e+30	> 4.576	7.73e+32	> 1.74e+33:	
RXJ0255.4+2005	900138	$0.043 \pm 0.025$	$0.232 \pm 0.032$	1.62 <sup>+0.29</sup> <sub>-0.30</sub>	< 1.37	1.98e+29	1.07e+30	4.395 $\pm$ 2.724	1.15e+33	3.19e+33	
LkH $\alpha$ 325	900193	$0.170 \pm 0.013$	$0.566 \pm 0.038$	0.47 <sup>+0.19</sup> <sub>-0.16</sub>	> 0.22	1.13e+31	7.54e+31	5.659 $\pm$ 0.627	1.92e+34	5.59e+34	
MEAN		$0.084 \pm 0.021$	$0.369 \pm 0.105$	$1.049 \pm 0.194$		2.51e+30	2.84e+31	$35.501 \pm 13.161$	2.48e+34	5.79e+34	
MEDIAN		0.047	0.241	0.792		8.35e+29	6.15e+30	5.192	3.70e+33	6.35e+33	

**Table 4.** Parameters derived from the lightcurves of flares detected on members of the Pleiades cluster in the *ROSAT* PSPC observations from Table 1. The last column gives the reference for flares that have been presented elsewhere in the literature: [a] Gagné et al. (1995), but newly reduced here. In the last two rows we give the mean (determined by taking account of lower/upper limits) and the median for each parameter.

Desig.	ROR	$I_{\text{qui}}$ [cps]	$I_{\text{max}}$ [cps]	$\tau_{\text{dec}}$ [h]	$\tau_{\text{ris}}$ [h]	$L_{\text{qui}}$ [erg/s]	$L_{\text{max}}$ [erg/s]	$L_{\text{F}}/L_{\text{qui}}$	$E_{\text{qui}}$ [erg]	$E_{\text{F}}$ [erg]	Notes
hii2147	200008-2	$0.130 \pm 0.017$	$1.041 \pm 0.017$	0.52	< 3.13	$9.52\text{e}+29$	$1.52\text{e}+31$	$15.015 \pm 1.985$	$1.78\text{e}+33$	$1.59\text{e}+34$	
hii1384	200008-2	$0.063 \pm 0.010$	$0.211 \pm 0.027$	$0.34^{+3.03}_{-0.19}$	> 0.22	$9.22\text{e}+29$	$3.09\text{e}+30$	$2.349 \pm 0.590$	$1.13\text{e}+33$	$1.66\text{e}+33$	
hii298	200068-1	$0.052 \pm 0.024$	$0.180 \pm 0.032$	$1.28^{+0.82}_{-0.54}$	> 0.00	$3.81\text{e}+29$	> $2.64\text{e}+30$	> 5.923	$1.75\text{e}+33$	> $5.43\text{e}+33$ :	
hii303	200068-1	$0.085 \pm 0.027$	$0.236 \pm 0.039$	$1.17^{+0.81}_{-1.01}$	3.12	$6.22\text{e}+29$	$3.45\text{e}+30$	$4.553 \pm 1.742$	$2.62\text{e}+33$	$5.92\text{e}+33$	
hcg307	200068-1	$0.004 \pm 0.007$	$0.163 \pm 0.025$	$0.50^{+0.23}_{-0.24}$	0.22	$5.86\text{e}+28$	$2.39\text{e}+30$	$39.750 \pm 69.865$	$1.05\text{e}+32$	$2.64\text{e}+33$	
hii1100	200068-1	$0.019 \pm 0.009$	$0.107 \pm 0.023$	$0.83^{+0.69}_{-0.49}$	1.48	$1.39\text{e}+29$	$1.57\text{e}+30$	$10.263 \pm 5.452$	$4.16\text{e}+32$	$2.43\text{e}+33$	[a]
hcg144	200068-1	$0.018 \pm 0.016$	$0.407 \pm 0.046$	$0.56^{+0.14}_{-0.13}$	4.58	$2.64\text{e}+29$	> $5.96\text{e}+30$	> 21.611	$5.31\text{e}+32$	> $7.24\text{e}+33$ :	
hii2244	200556	$0.029 \pm 0.013$	$0.149 \pm 0.013$	3.49	< 1.64	$4.25\text{e}+29$	> $2.18\text{e}+30$	> 4.138	$5.33\text{e}+33$	> $1.39\text{e}+34$ :	
hcg422	200556	$0.003 \pm 0.004$	$0.041 \pm 0.009$	< 1.56	1.61	$4.39\text{e}+28$	$6.00\text{e}+29$	$12.667 \pm 17.205$	$2.47\text{e}+32$	< $1.97\text{e}+33$ :	
hii1516	200556	$0.028 \pm 0.019$	$0.714 \pm 0.071$	$1.22^{+0.15}_{-0.16}$	< 1.64	$4.10\text{e}+29$	> $1.05\text{e}+31$	> 24.500	$1.80\text{e}+33$	> $2.78\text{e}+34$ :	[a]
hcg97	200557	$0.003 \pm 0.005$	$0.063 \pm 0.015$	$0.88^{+0.50}_{-0.39}$	1.44	$4.39\text{e}+28$	$9.22\text{e}+29$	$20.000 \pm 33.747$	$1.39\text{e}+32$	$1.77\text{e}+33$	[a]
hii1653	200557	$0.034 \pm 0.019$	$0.176 \pm 0.039$	$0.40^{+1.21}_{-0.22}$	< 1.16	$4.98\text{e}+29$	$2.58\text{e}+30$	$4.176 \pm 2.660$	$7.17\text{e}+32$	$1.91\text{e}+33$	
hii174	200557	$0.038 \pm 0.014$	$0.153 \pm 0.023$	$1.12^{+0.30}_{-0.28}$	< 3.31	$5.56\text{e}+29$	$2.24\text{e}+30$	$3.026 \pm 1.321$	$2.24\text{e}+33$	$4.28\text{e}+33$	[a]
hii191	200557	$0.004 \pm 0.004$	$0.119 \pm 0.021$	$0.99^{+0.21}_{-0.19}$	< 1.70	$5.86\text{e}+28$	$1.74\text{e}+30$	$28.750 \pm 29.243$	$2.09\text{e}+32$	$3.79\text{e}+33$	[a]
hii253	200557	$0.107 \pm 0.025$	$0.213 \pm 0.030$	$1.44^{+0.70}_{-0.56}$	> 0.00	$1.57\text{e}+30$	> $3.12\text{e}+30$	> 0.991	$8.12\text{e}+33$	> $5.07\text{e}+33$ :	
hii212	200557	$0.005 \pm 0.005$	$0.053 \pm 0.014$	$1.07^{+0.68}_{-0.50}$	< 1.44	$7.32\text{e}+28$	> $7.76\text{e}+29$	> 9.600	$2.82\text{e}+32$	> $1.72\text{e}+33$ :	[a]
hii345	200557	$0.055 \pm 0.013$	$0.176 \pm 0.027$	$0.63^{+0.39}_{-0.48}$	< 1.32	$8.05\text{e}+29$	$2.58\text{e}+30$	$2.200 \pm 0.753$	$1.83\text{e}+33$	$2.53\text{e}+33$	[a]
hcg181	200557	$0.009 \pm 0.007$	$0.128 \pm 0.021$	$0.70^{+0.32}_{-0.30}$	0.33	$1.32\text{e}+29$	$1.87\text{e}+30$	$13.222 \pm 10.574$	$3.32\text{e}+32$	$2.77\text{e}+33$	[a]
sk702	200557	$0.010 \pm 0.009$	$0.138 \pm 0.009$	0.10	1.27	$1.46\text{e}+29$	$2.02\text{e}+30$	$12.800 \pm 11.590$	$5.27\text{e}+31$	$4.39\text{e}+32$	
hcg143	200557	$0.011 \pm 0.009$	$0.217 \pm 0.030$	$0.36^{+0.23}_{-0.14}$	0.11	$1.61\text{e}+29$	$3.18\text{e}+30$	$18.727 \pm 15.585$	$2.09\text{e}+32$	$2.47\text{e}+33$	[a]
MEAN		$0.035 \pm 0.008$	$0.234 \pm 0.052$	$0.919 \pm 0.156$		$4.13 \text{e}+29$	$5.33\text{e}+30$	$16.792 \pm 3.059$	$1.49\text{e}+33$	$3.73\text{e}+33$	
MEDIAN		0.019	0.163	0.762		$2.64\text{e}+29$	$2.51\text{e}+30$	12.996	$5.31\text{e}+32$	$2.50\text{e}+33$	

**Table 5.** Parameters derived from the lightcurves of flares detected on members of the Hyades cluster in the *ROSAT* PSPC observations from Table 1. No analysis of flares on Hyads are reported in the literature. In the last two rows we give the mean (determined by taking account of lower/upper limits) and the median for each parameter.

Desig.	ROR	$I_{\text{qui}}$ [cps]	$I_{\text{max}}$ [cps]	$\tau_{\text{dec}}$ [h]	$\tau_{\text{ris}}$ [h]	$L_{\text{qui}}$ [erg/s]	$L_{\text{max}}$ [erg/s]	$L_{\text{F}}/L_{\text{qui}}$	$E_{\text{qui}}$ [erg]	$E_{\text{F}}$ [erg]	Notes
V471Tau	200107-0	$0.796 \pm 0.062$	$1.135 \pm 0.062$	0.10	< 5.87	$1.90\text{e}+30$	$2.70\text{e}+30$	$0.426 \pm 0.115$	$6.83\text{e}+32$	$1.75\text{e}+32$	
VB50	200441	$0.379 \pm 0.082$	$0.975 \pm 0.101$	0.47 <sup>+0.17</sup> <sub>-0.14</sub>	0.22	$4.16\text{e}+29$	$2.14\text{e}+30$	$4.145 \pm 1.065$	$7.03\text{e}+32$	$1.41\text{e}+33$	
VA677	200553	$0.333 \pm 0.071$	$0.493 \pm 0.080$	2.38 <sup>+1.68</sup> <sub>-0.87</sub>	< 327.6	$5.89\text{e}+29$	> $1.74\text{e}+30$	>1.961	$5.04\text{e}+33$	> $3.07\text{e}+33$ :	
LP357-4	200556	$0.152 \pm 0.029$	$0.345 \pm 0.034$	3.75 <sup>+1.75</sup> <sub>-1.15</sub>	> 0.22	$3.54\text{e}+29$	$8.05\text{e}+29$	$1.270 \pm 0.381$	$4.79\text{e}+33$	$3.83\text{e}+33$	
VA275	200776	$0.055 \pm 0.028$	$0.474 \pm 0.028$	<0.42	< 0.22	$1.28\text{e}+29$	$1.11\text{e}+30$	$7.618 \pm 3.945$	$1.94\text{e}+32$	< $9.30\text{e}+32$ :	
VB141	200777	$0.747 \pm 0.055$	$1.040 \pm 0.078$	1.44 <sup>+0.76</sup> <sub>-0.53</sub>	< 1.20	$1.86\text{e}+30$	> $2.60\text{e}+30$	>0.392	$9.67\text{e}+33$	> $2.39\text{e}+33$ :	
VA334	200777	$0.137 \pm 0.021$	$0.329 \pm 0.021$	<1.39	0.33	$2.51\text{e}+29$	> $6.02\text{e}+29$	>1.401	$1.25\text{e}+33$	$1.11\text{e}+33$ :	
VB141	200777	$0.747 \pm 0.055$	$1.003 \pm 0.075$	0.75 <sup>+0.95</sup> <sub>-0.37</sub>	< 1.32	$1.86\text{e}+30$	$2.50\text{e}+30$	$0.343 \pm 0.127$	$5.03\text{e}+33$	$1.09\text{e}+33$	
VA334	200777	$0.137 \pm 0.021$	$0.309 \pm 0.021$	0.75	< 1.64	$2.51\text{e}+29$	$5.65\text{e}+29$	$1.255 \pm 0.290$	$6.76\text{e}+32$	$5.41\text{e}+32$	
VA677	200911	$0.282 \pm 0.056$	$0.896 \pm 0.083$	0.46 <sup>+0.26</sup> <sub>-0.16</sub>	< 1.61	$4.98\text{e}+29$	$3.17\text{e}+30$	$5.355 \pm 1.232$	$8.25\text{e}+32$	$2.26\text{e}+33$	
VA677	200945	$0.238 \pm 0.036$	$0.474 \pm 0.073$	0.22 <sup>+0.34</sup> <sub>-0.11</sub>	< 4.59	$4.21\text{e}+29$	> $1.68\text{e}+30$	>2.983	$3.33\text{e}+32$	> $4.26\text{e}+32$ :	
VB169	201097	$0.110 \pm 0.025$	$0.251 \pm 0.025$	0.18	< 1.67	$2.59\text{e}+29$	$5.90\text{e}+29$	$1.282 \pm 0.434$	$1.68\text{e}+32$	$1.35\text{e}+32$	
VA673	201313	$0.409 \pm 0.022$	$0.975 \pm 0.066$	1.78 <sup>+0.48</sup> <sub>-0.35</sub>	> 0.13	$4.77\text{e}+29$	> $2.27\text{e}+30$	>3.768	$3.06\text{e}+33$	> $5.35\text{e}+33$ :	
VB190	201368	$0.165 \pm 0.061$	$0.472 \pm 0.061$	0.20	< 20.52	$1.92\text{e}+29$	$1.10\text{e}+30$	$4.721 \pm 1.931$	$1.39\text{e}+32$	$3.33\text{e}+32$	
VB141	201368	$0.985 \pm 0.136$	$6.897 \pm 0.183$	1.21 <sup>+0.16</sup> <sub>-0.18</sub>	< 1.14	$2.46\text{e}+30$	$1.72\text{e}+31$	$6.002 \pm 0.860$	$1.07\text{e}+34$	$4.08\text{e}+34$	
VB85	201368	$0.209 \pm 0.027$	$0.396 \pm 0.027$	<1.91	> 0.55	$3.86\text{e}+29$	> $7.31\text{e}+29$	>0.895	$2.65\text{e}+33$	$1.50\text{e}+33$ :	
VB45	201369	$0.034 \pm 0.020$	$0.167 \pm 0.020$	0.37	< 0.98	$4.12\text{e}+28$	> $4.05\text{e}+29$	>8.824	$5.49\text{e}+31$	> $2.72\text{e}+32$ :	
MEAN		$0.348 \pm 0.069$	$0.978 \pm 0.367$	$0.902 \pm 0.234$		$7.26\text{e}+29$	$4.24\text{e}+30$	$4.433 \pm 0.767$	$2.71\text{e}+33$	$5.62\text{e}+33$	
MEDIAN		0.223	0.473	0.463		$4.01\text{e}+29$	$2.34\text{e}+30$	4.468	$7.64\text{e}+32$	$8.17\text{e}+32$	

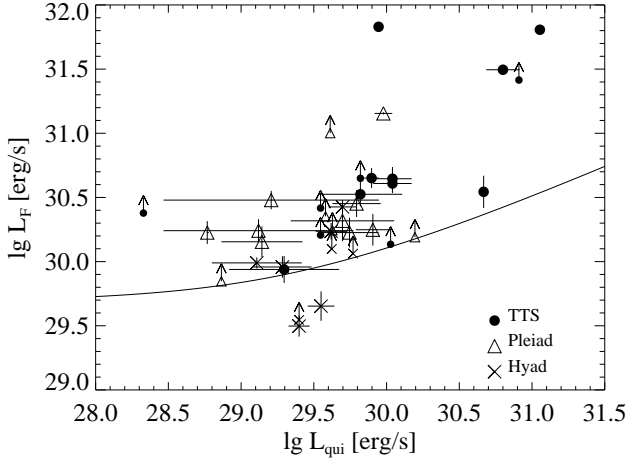


**Fig. 5.** Correlation between quiescent and flare luminosity. TTSs, Pleiads, and Hyads are represented by different plotting symbols: TTS – circles, Pleiads – triangles, Hyads – crosses. The solid curve is the minimum flare strength needed for detection of a flare with given  $L_{\text{qui}}$  if the star is at a distance of 140 pc. The data points below that curve represent no contradiction to the calculated threshold because the detection threshold increases with stellar distance, i.e. apparent brightness of the stars, and therefore Pleiads and Hyads may show flares with smaller  $L_F$  for given  $L_{\text{qui}}$ .

time bin. (In our actual flare search we were even more conservative; see Sect. 4.) Hypothetical events of that kind obey a detection threshold curve for  $L_F/L_{\text{qui}}$  as shown in Fig. 6. As mentioned above, the minimum flare luminosity needed for detection of a flare becomes larger with increasing quiescent brightness. In contrast, the required luminosity ratio, i.e. the relative strength of the events, decreases when  $I_{\text{qui}}$  increases. Note also, that the curve in Fig. 6 is distance independent. But the relation between  $L_{\text{qui}}$  and the corresponding minimum  $L_F$  of a detectable flare differs for stars at different distances. In Fig. 5 we have overplotted the theoretical threshold for detection of a flare on a star at 140 pc distance. Note, that the slope of the data in Fig. 5 is somewhat steeper than the increase of the threshold imposed by the S/N. This seems to indicate an intrinsic correlation between quiescent and flare luminosity. We have subtracted the theoretical threshold value for  $L_F$  from the observed flare luminosity for each of the stars from Fig. 5. Correlation tests for the difference between threshold and observed value for  $L_F$ ,  $(L_{F,\text{theo}} - L_{F,\text{obs}})$ , with  $L_{\text{qui}}$  show that the correlation is of low significance,  $\alpha=0.05$ . The data points below the theoretical curve are all Pleiads or Hyads. They do not contradict the threshold curve, since Pleiades and Hyades stars are closer than 140 pc and therefore have a lower flare detection threshold.

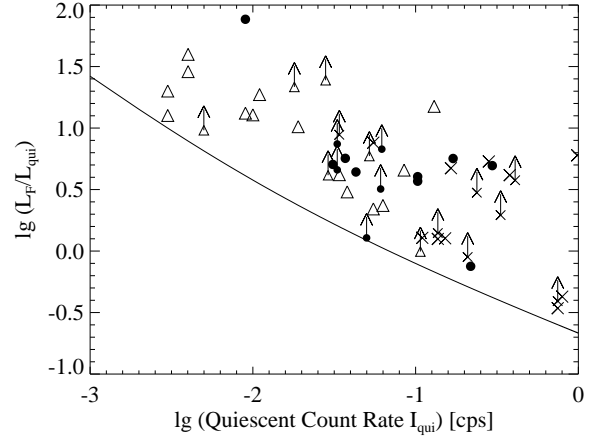


**Fig. 6.** Relative flare strength,  $L_F/L_{\text{qui}}$ , as a function of the quiescent count rate  $I_{\text{qui}}$  in double logarithmic scale. Assuming that the flare is characterized by a rise in count rate of  $3\sigma$  above the mean during a single 400 s time bin, the solid curve gives the minimum values of  $L_F/L_{\text{qui}}$  for which a flare will be detected on stars with given  $I_{\text{qui}}$ . The observed values consistently lie above this line. The meaning of the plotting symbols is the same as in Fig. 5. For clarity we have omitted error bars.

## 6. Statistical comparison of the flaring stars

We present now a statistical analysis of the X-ray flares from Tables 3, 4 and 5. A detailed discussion of the (quiescent) X-ray properties of all detected and undetected stars is postponed to a later paper (Stelzer et al., in preparation).

In this section, different flare parameters will be checked for dependence on age, circumstellar environment, and rotation rate (Sect. 6.2, 6.3, 6.4.) to see whether any of these properties has an effect on the characteristic luminosity and time scales of coronal activity. For the statistical comparison of the flaring stars the ASURV package version 1.2 (Feigelson & Nelson 1985) was used.

First we compare the flaring populations of TTSs, Pleiads, and Hyads concerning their effective temperatures. We have converted spectral types to effective temperatures using the conversion given in Kenyon & Hartmann (1995) for PMS stars earlier than M0, and Luhman (1999) for PMS M-type stars intermediate between dwarfs and giants. For Pleiades and Hyades stars we have used the conversion of Schmidt-Kaler (1982). We have applied two-sample tests to each pair of  $T_{\text{eff}}$ -distributions to reveal possible differences between flaring stars of the three groups. Henceforth, we denote the probability that the distributions are similar by  $\alpha$ . In all but one of the comparisons we found  $\alpha > 0.2$ , and therefore no significant differences in  $T_{\text{eff}}$ . The exception is the logrank test between TTSs and Hyads where  $\alpha = 0.03$ .

Most flares occurred on G, K and M stars. However, some events were observed on A and F stars. Stars of intermediate spectral type, lacking both a convection-driven dynamo and

**Table 6.** Results of two-sample tests between each pair of stellar samples (TTSs, Pleiads, and Hyads) with respect to the effective temperature  $T_{\text{eff}}$  of the flaring star. Only flares on G, K, or M stars have been admitted. The analysis was performed with the ASURV package. Next to the mean and median of  $T_{\text{eff}}$  we give the probability that the null hypothesis of two distributions being the same is true derived from Gehan’s generalized Wilcoxon test and the logrank test. The values suggest that there is no significant difference between the spectral types of the flaring TTSs, Pleiads, and Hyads and justify to combine G, K, and M stars for the comparison of flares from these different stellar groups.

Sample Name	Sample Size	$\lg T_{\text{eff}}$		Prob. GW (HV)	Prob. logrank
		MEAN	MED.		
TTSs	15	$3.63 \pm 0.08$	3.600	0.395	0.525
Pleiads	14	$3.66 \pm 0.07$	3.675		
				0.897	0.972
TTSs	15	(see above)		0.212	0.401
Hyads	11	$3.63 \pm 0.07$	3.595		
Pleiads	14	(see above)			
Hyads	11	(see above)			

a strong stellar wind, seem to have no efficient mechanism to generate X-ray flares. Therefore, it is often assumed that X-ray emission apparently seen on A or B stars, can be attributed to an (unknown) late-type companion (see e.g. Stauffer et al. 1994, Gagné & Caillault 1994, Panzera et al. 1999). The same arguments can be applied to explain X-ray flares on these stars. In any case, the emission mechanism of early-type stars is different from that of late-type stars. From the sharp onset of rotation-activity relations in dwarf stars Walter (1983) has argued that the onset of solar-like dynamo activity occurs abruptly at about spectral type F5. To ensure that no stars with X-ray generation mechanisms other than stellar dynamos are included, we have excluded the stars of spectral type F and earlier from the statistical analysis presented in this paper, i.e. we have restricted the flare sample to events on G, K, and M stars. This limitation provides samples which have similar  $T_{\text{eff}}$  distributions, i.e.  $\alpha > 0.2$  also for the two-sample test between TTSs and Hyads (see Table 6 for the detailed results). This justifies to combine all flaring late-type stars for the statistical analysis. In the following the stellar sample is restricted to G, K, and M stars. If not explicitly mentioned the two flares on known white-dwarf systems (on V471 Tau and VA 673) are excluded from the sample, since the white dwarf could be responsible for the X-ray event instead of its late-type companion.

### 6.1. Flare frequency of MS stars and spectral type

It is interesting to ask whether the depth of the convection zone has any influence on the occurrence of surface flares.

Since the relative size of the convection zone increases for later spectral types, the distribution of flares onto stars of different spectral types may help to solve this question. What we really want to check is whether the flare frequency depends on stellar mass, which corresponds to spectral type on the MS. Because PMS stars still evolve through the Hertzsprung-Russell diagram (HRD), i.e. change their spectral type, we exclude the TTSs from this part of the analysis. Flaring Pleiades and Hyades stars are combined to increase the sample size.

We have studied the spectral type distribution of flares by comparing the number of flares on stars of a certain spectral type to the total number of detected stars of that spectral type. The detection sensitivity for flares of a given strength  $L_F/L_{\text{qui}}$  is different for each star because it depends on the level of quiescent emission  $I_{\text{qui}}$  (see Sect. 5).  $I_{\text{qui}}$  depends on the spectral type of the star. For this reason, a simple comparison between numbers of flares and numbers of detected stars of each spectral type would be misleading. The observational bias can, however, be eliminated if the numbers (of flares and detections) are evaluated above a certain threshold  $L_F/L_{\text{qui}}$ . We compare the number of flares with measured luminosity ratio above a critical value  $(L_F/L_{\text{qui}})_{\text{crit}}$  to the number of detected stars for which  $I_{\text{qui}}$  exceeds the minimum value needed for detection of a flare of that critical strength. We have compiled these numbers for a reasonable range of values  $L_F/L_{\text{qui}}$ , and show the result in Fig. 7. Plotted are the number of flares exceeding  $L_F/L_{\text{qui}}$  divided by the number of detected stars that are bright enough for detection of flares with that value of  $L_F/L_{\text{qui}}$ . G stars clearly show the smallest rate of events throughout all of the observed range of flare strengths.

### 6.2. Age of flaring stars (Luminosity functions)

To study how the flare activity of young late-type stars evolves with stellar age we have computed luminosity distribution functions (LDF) and performed two-sample tests for three sub-samples of stars: TTSs, Pleiads, and Hyads.

Maximum likelihood distributions for TTSs, Pleiads, and Hyads are presented in Fig. 8 for both flare luminosity  $L_F$  and mean luminosity during the *quiescent* part of flare observations  $L_{\text{qui}}$ . Note, that Fig. 8 (b) contains no upper limits because only stars which have shown a flare are included, and  $L_{\text{qui}}$  during flare observations can be extracted from the lightcurves. The flare luminosity in Fig. 8 (a) includes upper limits. Since  $L_F = L_{\text{max}} - L_{\text{qui}}$ , upper limits for  $L_{\text{max}}$  (see Table 3, 4, and 5) translate to upper limits for  $L_F$ . LDFs for all non-flaring stars (detections and non-detections) will be shown elsewhere (Stelzer et al., in preparation).

Two-sample tests were applied to each pair of LDFs to search for differences. The results are given in Table 7 (for  $L_F$  and  $L_{\text{qui}}$ ). The null hypothesis of two samples being the same is rejected for all pairs of flare luminosity distributions at significance levels  $\alpha < 0.05$ . The quiescent luminosity of *flaring* TTSs is different from both the quiescent luminosity of *flaring* Pleiads and *flaring* Hyads. Usually the quiescent luminosity functions of Pleiades and Hyades stars are also found to

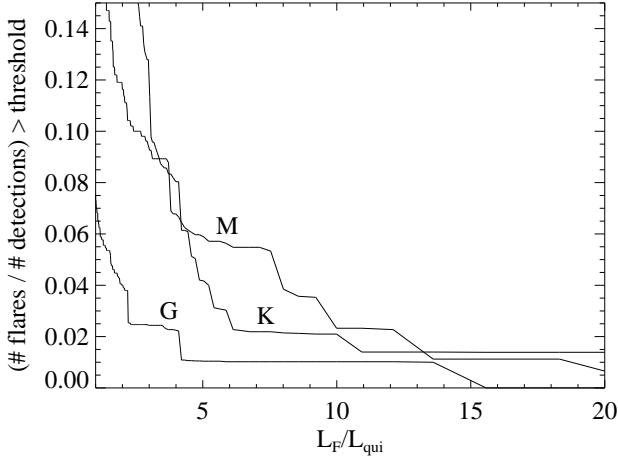


**Fig. 7.** Fraction of flares among detected stars above a given threshold  $L_F/L_{\text{qui}}$  for different spectral types. Shown are G stars (dashed line), K stars (solid line) and M stars (dotted line). Pleiades and Hyades stars have been combined. TTSs are not considered since they are on the PMS where the relation between the stellar interior structure and the X-ray emission might be different. Throughout the examined range of  $L_F/L_{\text{qui}}$  the number of flares per detected stars is lowest for spectral type G.

**Table 7.** Results of two-sample tests for the flare luminosity  $L_F$  and quiescent luminosity of flare observations  $L_{\text{qui}}$ . The number of upper limits to the luminosity are listed in brackets in column ‘Sample Size’. See Table 6 for the meaning of the remaining columns. All distributions of  $L_F$  are significantly different from each other. Flaring Pleiads and Hyads have similar  $L_{\text{qui}}$  distributions.

Sample Names	Sample sizes	Prob. GW	Prob logrank
Flare luminosity $L_F$			
TTSs - Pleiads	15(6) 14(5)	0.021	0.017
TTSs - Hyads	15(6) 9(3)	0.001	0.000
Pleiads - Hyads	14(5) 9(3)	0.007	0.010
Quiescent luminosity of flaring stars $L_{\text{qui}}$			
TTSs - Pleiads	15(0) 14(0)	0.025	0.010
TTSs - Hyads	15(0) 9(0)	0.007	0.001
Pleiads - Hyads	14(0) 9(0)	0.615	0.243

be distinct (see e.g. Caillault 1996). However, we find no difference ( $\alpha > 0.61$ ) between the quiescence luminosities of the flaring stars in these two clusters. Using the relation between  $I_{\text{qui}}$  and the threshold for  $L_F/L_{\text{qui}}$  (see Fig. 6) we have determined that more than 90% of the detected Hyades stars are bright enough for detection of a flare whose strength  $L_F/L_{\text{qui}}$  is equal to the mean observed for flares on late-type Hyads, i.e.  $L_F/L_{\text{qui}} = 4.527$ . The fact that mostly X-ray bright Hyades stars display flaring activity is therefore not a selection effect.

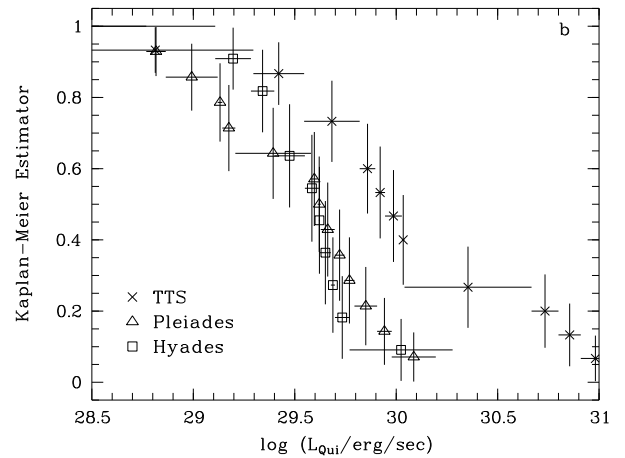
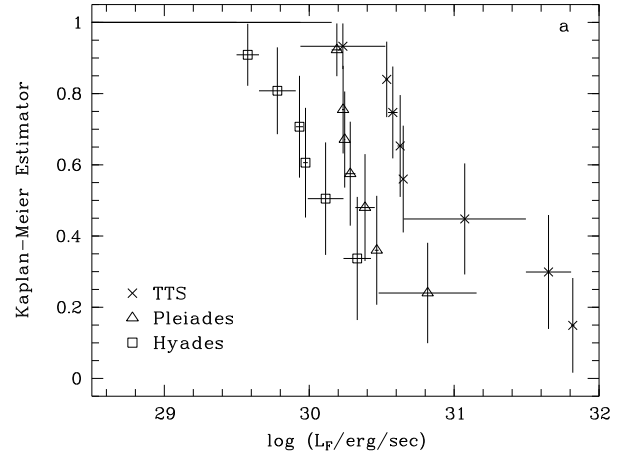


**Fig. 8.** Luminosity functions for the flaring TTSs, Pleiads, and Hyads during the X-ray flare (a) and during quiescence (b). Stars of spectral type earlier than G or unknown spectral type, and known white-dwarf systems are excluded. Note that the quiescent distribution of the Hyades stars is consistent with that of the Pleiads, due to the selection of flaring stars only (see discussion in the text).

Instead, flaring Hyads indeed are overluminous compared to the non-flaring Hyades stars detected by the *ROSAT* PSPC.

The mean luminosities of TTSs, Pleiads, and Hyads and their standard deviations derived with inclusion of upper limits are given in Table 8.

### 6.3. Flaring cTTSs and wTTSs

So far we have not distinguished between cTTSs and wTTSs, because it is a matter of debate whether all cTTSs are younger than wTTSs. However, they are clearly distinguished by their circumstellar environment. The disks of cTTSs may influence



**Table 8.** Mean and median flare and quiescent luminosity of flaring TTSs, Pleiads, and Hyads. The sample of cTTSs was too small to compute the median of  $L_F$ .

Sample Name	Sample Size	Mean	Median
Flare Luminosity $\lg L_F$			
TTSs	15 (6)	$31.05 \pm 0.19$	30.65
Pleiads	14 (5)	$30.51 \pm 0.12$	30.30
Hyads	9 (3)	$30.06 \pm 0.11$	29.99
cTTSs	6 (4)	$31.44 \pm 0.32$	—
wTTSs	8 (1)	$30.81 \pm 0.22$	30.58
Quiescent Luminosity of Flaring Stars $\lg L_{\text{qui}}$			
TTSs	15 (0)	$29.98 \pm 0.17$	29.92
Pleiads	14 (0)	$29.52 \pm 0.11$	29.61
Hyads	9 (0)	$29.50 \pm 0.07$	29.47
cTTSs	6 (0)	$29.94 \pm 0.19$	29.82
wTTSs	8 (0)	$30.22 \pm 0.19$	30.04

**Table 9.** Results of two-sample tests for differences between cTTSs and wTTSs with respect to the flare parameters  $L_{\text{qui}}$ ,  $L_F$ ,  $\tau_{\text{dec}}$ , and  $L_F/L_{\text{qui}}$ . The flare on the unresolved stars DD Tau/CZ Tau is not considered here, since it is not clear whether the event should be attributed to the wTTS (CZ Tau) or to the cTTS (DD Tau). The meaning of columns 2–5 is the same as in Table 7.

Parameter	Sample Size		Prob. GW	Prob logrank
	cTTSs	wTTSs		
$\lg L_F$	6(4)	8(1)	0.053	0.046
$\lg L_{\text{qui}}$	6(0)	8(0)	0.206	0.264
$\tau_{\text{dec}}$	6(2)	8(1)	0.714	0.752
$L_F/L_{\text{qui}}$	6(4)	8(1)	0.007	0.002

flare activity. We have, therefore, compared cTTSs and wTTSs with respect to several flare parameters (see Table 9 for the results). Significant differences are found in the flare luminosity  $L_F$  and relative strength of the flare  $L_F/L_{\text{qui}}$ . The decay timescale does not depend on the type of TTS. The values given in Table 9 have been derived from all flares on TTSs except the one on DD Tau/CZ Tau. DD Tau is a cTTS binary and CZ Tau a wTTS binary. The four stars are not resolved in the PSPC image. It is therefore impossible to classify this flare concerning the type of TTS. We have performed two further series of two-sample tests in which the event is included. In one of these series of tests the flare is attributed to DD Tau, and the other time to CZ Tau. The significance of the results did not change.

The mean flare and quiescent luminosities of cTTSs and wTTSs are given in Table 8. cTTSs, although characterized by lower quiescent emission, show stronger flares than wTTSs.

#### 6.4. $v \sin i$ of the flaring stars

Stellar rotation is one of the necessary conditions for magnetic activity. We have, therefore, examined the influence of the stellar rotation rate on the characteristics of X-ray flares. The relation between flare parameters and projected rotational velocity,  $v \sin i$ , is shown in Fig. 9. The statistical significance for cor-

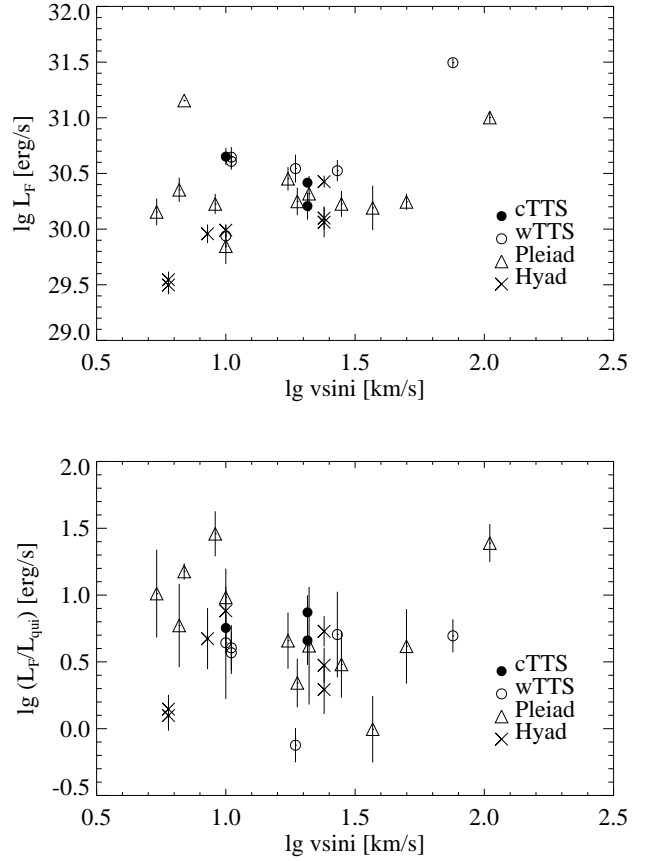


**Fig. 9.** X-ray luminosities versus projected rotational velocity  $v \sin i$  in double logarithmic scale: *top* - flare luminosity  $L_F$ , *bottom* - luminosity ratio  $L_F/L_{\text{qui}}$ . While  $L_F$  and  $v \sin i$  may show a weak positive correlation,  $L_F/L_{\text{qui}}$  does not depend on the rotation.

relations between some flare parameters and  $v \sin i$  is given in Table 10 (columns 2 and 3). The weak correlation between luminosity, both  $L_F$  and  $L_{\text{qui}}$ , and  $v \sin i$  is significant. The decay time  $\tau_{\text{dec}}$  and the relative flare strength  $L_F/L_{\text{qui}}$ , on the other hand, are not related to  $v \sin i$ .

We have studied the flaring population in terms of differences in flare characteristics between slow and fast rotators. The boundary was set to 20 km/s because this choice gives two samples of about equal size: 16 slow and 12 fast rotators showed an X-ray flare. Stars from Tables 3, 4, and 5 for which no measurement of  $v \sin i$  is available are ignored. The result of two sample tests for the parameters  $L_F$ ,  $L_{\text{qui}}$ ,  $\tau_{\text{dec}}$ , and  $L_F/L_{\text{qui}}$  are presented in the remaining columns of Table 10. In no case the null hypothesis that slow and fast rotators are drawn from the same distribution was rejected at significance level  $\alpha < 0.05$ .

**Table 10.** Relation between flare parameters  $L_{\text{qui}}$ ,  $L_{\text{F}}$ ,  $\tau_{\text{dec}}$ , and  $L_{\text{F}}/L_{\text{qui}}$  and the projected rotational velocity  $v \sin i$ : Columns 2 and 3 are results of correlation tests between each of the listed parameters and  $v \sin i$ . The remaining columns give results of two-sample tests for differences between slow and fast rotators with boundary at 20 km/s. The samples consist of 16 slow versus 12 fast rotators.

Parameter	Pearson r (Signif.)	Spearman r (Signif.)	Prob. GW	Prob logrank
$\lg L_{\text{F}}$	0.479 (0.005)	0.372 (0.026)	0.075	0.091
$\lg L_{\text{qui}}$	0.468 (0.006)	0.496 (0.004)	0.269	0.528
$\tau_{\text{dec}}$	0.247 (0.103)	0.221 (0.129)	0.487	0.584
$L_{\text{F}}/L_{\text{qui}}$	-0.017 (0.466)	-0.287 (0.069)	0.399	0.547

## 7. Flare rates

In this section, we will derive flare rates as a means to determine the activity level for a stellar sample with distinct properties. The characteristic properties which will be examined are (a) stellar age (comparing TTSSs, Pleiads, and Hyads), (b) stellar rotation (comparing slow and fast rotators), and (c) stellar multiplicity (comparing close binaries to other stars). Flare rates will be computed separately for each group of stars.

We assume that the duration of the active state is represented by the decay timescale  $\tau_{\text{dec}}$ , i.e. the generally poorly restricted rise times  $\tau_{\text{ris}}$  are neglected. This is certainly wrong for the flare on hcg 144 which seems to have a somehow reversed character (slow rise and rapid decay). However, hcg 144 is a star of unknown spectral type and therefore not part of the group to be examined here. To compile the flare rates,  $F = \sum (\tau_i)/T_{\text{obs}}$ , we have added up the decay timescales  $\tau_{\text{dec}}$  of the flares and divided this sum by the total observing time,  $T_{\text{obs}}$ , of all detections (flaring and non-flaring stars). Only the nearest identification of each X-ray source has been considered in the compilation of  $T_{\text{obs}}$ . But for multiple systems we have multiplied the observing time by the number of components. For the compilation of  $T_{\text{obs}}$  we have eliminated data gaps larger than 1 h, the typical flare duration. This provides us the fraction of the total observing time during which the stars are observed in the active state.

In practice  $\sum (\tau_i)$  is computed from the sample mean  $\bar{\tau}$  returned by ASURV's Kaplan-Meier estimator. This way we ensure that upper limits to  $\tau_{\text{dec}}$  are taken into account. The Kaplan-Meier estimator returns also the uncertainty of  $\bar{\tau}$ . To include the spread of the data in the estimation of  $F$  we have converted this uncertainty of the mean to the sample variance  $\sigma_{\tau}$ . Consequently:

$$F = \frac{\bar{\tau} \cdot N}{T_{\text{obs}}} \pm \frac{\sigma_{\tau} \cdot \sqrt{N}}{T_{\text{obs}}} \quad (1)$$

### 7.1. Flare rate and stellar age

The evolution of flare rates with stellar age is examined by comparing the flare frequency of TTSSs to that of the Pleiades and the Hyades. 15 flares have occurred on TTSSs, 14 on late-

type Pleiads, and 11 on late-type Hyads. We have derived the following values for the flare rate  $F$ :  $0.86 \pm 0.16\%$  (TTSSs),  $0.67 \pm 0.13\%$  (Pleiads), and  $0.86 \pm 0.32\%$  (Hyads). When the white-dwarf binaries are excluded the flare rate for Hyades declines to  $F_{\text{H,noWD}} = 0.71 \pm 0.30\%$ .

The flare rates are biased for several reasons which will be explained next. First, the flare detection limit is determined by the S/N, which in turn depends on the distance to the star. Therefore, flare rates of TTSSs, Pleiads, and Hyads are only comparable above a limiting minimum strength of the flare, expressed by a threshold  $L_{\text{F}}/L_{\text{qui}}$ . And, secondly, incomplete data sampling might lead to wrong conclusions about the decay timescale of individual events and thus contaminate the resulting  $F$ .

To solve the first problem we have scaled the quiescent count rate of all flaring stars to a distance of 140 pc, the distance of most of the TTSSs. I.e. we have multiplied all quiescent count rates with a factor  $(\frac{d}{140 \text{ pc}})^2$ . These theoretical values of  $I_{\text{qui}}$  correspond to higher flare detection thresholds  $L_{\text{F}}/L_{\text{qui}}$  for all stars except the ones in Perseus. All flares from Perseus stars would be detected at 140 pc, since they are further away than this distance. The observed luminosity ratios of all flaring stars have then been compared to the theoretical threshold needed if the star were at 140 pc. All flares for which the observed value is below this requirement should be neglected when the flare rates are computed. It turns out that all flares on Pleiads remain above the 140 pc threshold. But only 7 out of 11 flares on Hyads (one of the 7 is a white-dwarf system) have  $L_{\text{F}}/L_{\text{qui}}$  high enough to be detected at a distance of 140 pc. Now the comparison of our different samples is free from the sensitivity bias. And we derive flare rates  $F$  of  $0.86 \pm 0.16\%$  (TTSSs),  $0.67 \pm 0.13\%$  (Pleiads), and  $0.46 \pm 0.19\%$  (Hyads). Without the white-dwarf binary  $F$  decreases for the Hyades to  $0.32 \pm 0.17\%$ .

The uncertainties in the measurement of the flare duration are less easy to overcome. The large flare rate of TTSSs is partially due to two extraordinary long events of duration  $> 8$  h (see Table 3). The decay times of both of these flares are considered to be an upper limit. If these two events are discarded from the sample of flares,  $F_{\text{TTSS}} = 0.74 \pm 0.14\%$ .

We have also compiled  $F$  for cTTSSs and wTTSSs separately to see whether the circumstellar environment has any influence on the frequency of the flare activity. Among the events on TTSSs, 6 are observed on cTTSSs and 8 on wTTSSs. An additional flare was seen from the unresolved stars DD Tau/CZ Tau. The classification of this event within the subgroups of TTSSs remains therefore unclear, and complicates the comparison of  $F$  for the two classes of TTSSs. At first, the event on DD Tau/CZ Tau has been eliminated from the sample, thus that 6 flares on cTTSSs are opposed to 8 flares on wTTSSs. The respective flare rates are  $F_{\text{c}} = 1.09 \pm 0.39\%$  and  $F_{\text{w}} = 0.65 \pm 0.16\%$ . When the ambiguous event is counted on the side of the cTTSSs  $F_{\text{c}}$  rises to  $1.28 \pm 0.37\%$ . When it is attributed to the wTTSS CZ Tau instead,  $F_{\text{w}}$  becomes  $0.76 \pm 0.16\%$ . Note, that even though the number of flares on wTTSSs is higher than the number of flares on cTTSSs, the flare rate for wTTSSs is lower

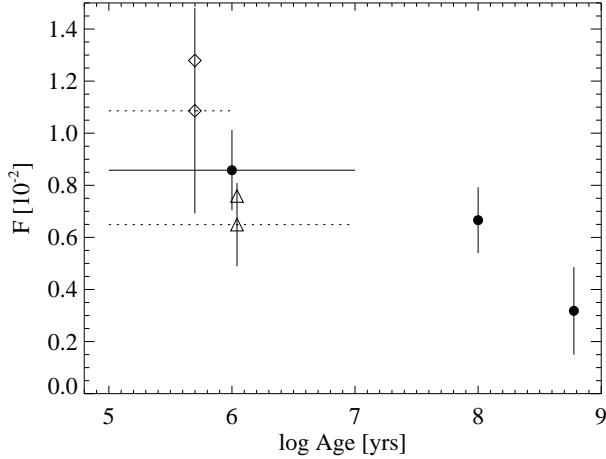


**Fig. 10.** Flare rate  $F = \sum(\tau_i)/T_{\text{obs}}$  as a function of stellar age for TTSS, Pleiads, and Hyads. To eliminate biases due to the S/N-dependence of the detection sensitivity for flares, only events which are bright enough for detection at a uniform distance of 140 pc are considered. Furthermore, flares which can not definitely be assigned to a late-type star are excluded. The flare rates for cTTSS (diamonds) and wTTSS (triangles) alone are overplotted. The upper of the two symbols applies if the ambiguous event on DD Tau/CZ Tau is included in the sample (see text). The horizontal bars represent the age spread of TTSS.

than the flare rate for cTTSS. This is possible because of differences in the total observing time.

$F$  as a function of stellar age is displayed in Fig. 10. The decline of the flare rate with stellar age is obvious. Rates for cTTSS and wTTSS are symbolized by diamonds and triangles, respectively. The location of the lower diamond and triangle describes the flare rates without the event on DD Tau/CZ Tau. The upper diamond and triangle are values for  $F$  if this flare is included in the respective group of TTSS.

### 7.2. Flare rate and rotational velocity

Here we examine whether the flare frequency depends on rotation. This is done by computing  $F$  (defined as before) for fast rotators on the one hand ( $v \sin i > 20$  km/s) and slow rotators on the other hand ( $v \sin i < 20$  km/s). Again, only late-type stars are considered. The resulting rates are  $F_{\text{slow}} = 0.55 \pm 0.10\%$  and  $F_{\text{fast}} = 1.55 \pm 0.38\%$ . Thus there is a clear trend towards an increase of flare activity with increasing rotational velocity.

### 7.3. Flare rate and multiplicity

Another interesting question is whether the circumstellar surroundings have any influence on the flare frequency. The coronal activity may e.g. change if there are interactions between

the magnetic fields of binaries. Such interactions are expected to take place only in *close* binaries. To search for such a connection we, therefore, discriminate between spectroscopic binaries on the one hand and all others, i.e. singles or visual multiples. The flare rate  $F$  is computed in the same way as before. Since the observation time of each stellar system has been multiplied by the number of components, the flare rates should be about equal for both samples if the underlying physics are the same. However, we find that the flare rate of spectroscopic binaries is enhanced by more than a factor of two:  $F_{\text{non-SB}} = 0.64 \pm 0.12\%$  and  $F_{\text{SB}} = 1.43 \pm 0.25\%$ . Note, that the study of individual flare parameters (similar to the analysis of Sect. 6) has shown no difference for these two samples.

## 8. Hardness Ratios

For most of the flaring sources not enough counts are collected by the PSPC to compare the different levels of X-ray emission in a detailed spectral analysis. Therefore, we use hardness ratios to mark spectral changes. *ROSAT* PSPC hardness ratios are defined by:

$$HR1 = \frac{H - S}{H + S} \quad HR2 = \frac{H_2 - H_1}{H_2 + H_1} \quad (2)$$

where  $S$ ,  $H$ ,  $H_1$ , and  $H_2$  denote the count rates in the *ROSAT* PSPC soft (0.1-0.4 keV), hard (0.5-2.0 keV), hard1 (0.5-0.9 keV) and hard2 (0.9-2.0 keV) band respectively. For each flare observation  $HR1$  and  $HR2$  are computed for three activity stages representing the quiescent state (pre- and post-flare), the rise and the decay, respectively. Sometimes no counts are measured in one or more of the energy bands. Whenever this is the case we have derived upper limits for the hardness ratio making use of the background counts in that energy band at the source location.

The observed hardness ratios,  $HR1$  and  $HR2$ , are plotted in Fig. 11. The plots comparing quiescent and flare state show marginal evidence that most of the stars lie below the diagonal in the hardness plot (see lower left panel of Fig. 11) and thus are harder during the flare intervals as compared to their quiescence. No significant difference in hardness is observed between flare rise and flare decay. When impulsive heating takes place before the outburst the plasma cools quickly by radiation and conduction to the chromosphere. Therefore, the similar hardness observed during rise and decay phase suggests that heating takes place throughout the decay.

To quantify the differences in hardness between different flare stages we have computed mean hardness ratios for each of the stellar groups. In Table 11 we show the mean hardness for each activity stage (quiescence, rise, and decay) and each sample of stars (TTSS, Pleiads, and Hyads). The hardness changes systematically when the three groups are compared to each other: TTSS display the hardest spectra, followed by Pleiads, which in turn are characterized by higher hardness ratios than the Hyades stars. This is also manifest in the hardness plots of Fig. 11 where the three samples occupy different regions. In Sect. 6.2 it was shown that the flare luminosity declines with

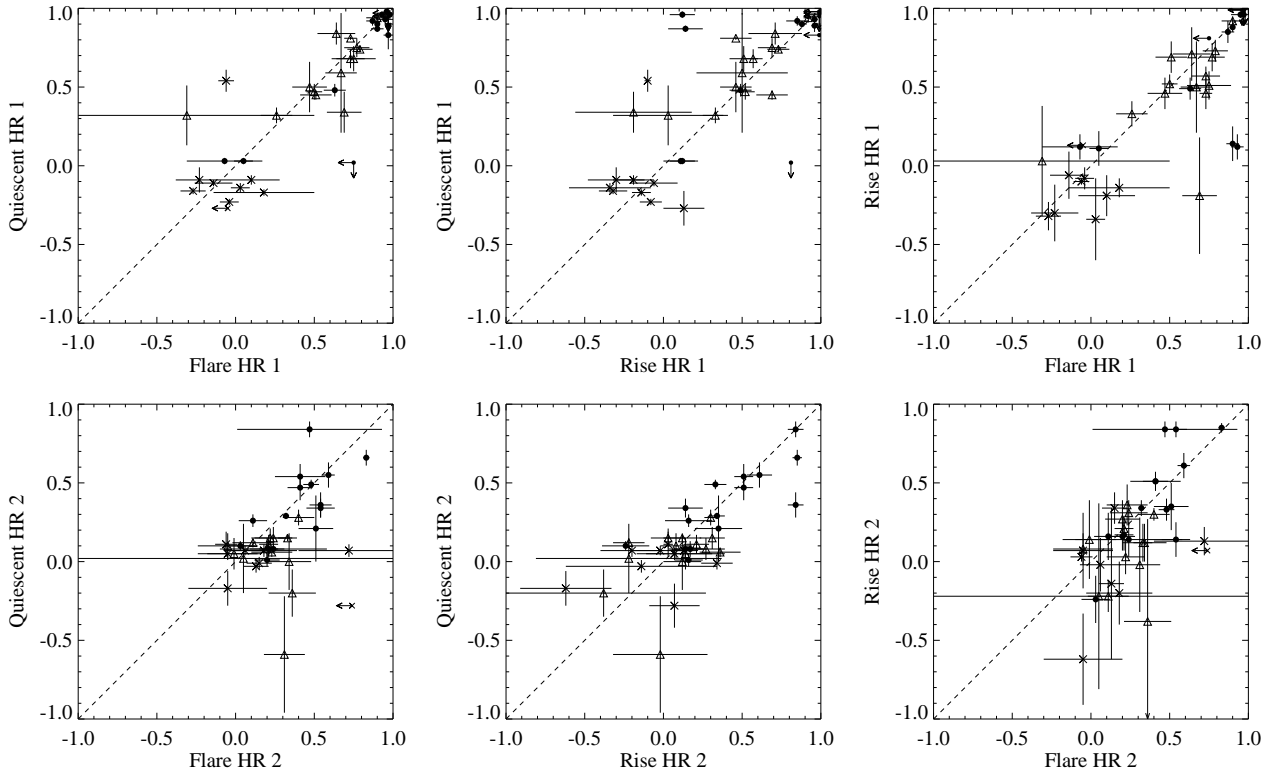


**Fig. 11.** Comparison of *ROSAT* PSPC hardness ratios for quiescent state, flare rise and flare decay of the late-type stars from Tables 3, 4, and 5. *top* - *HR 1*, *bottom* - *HR 2*. The meaning of the plotting symbols is the same as in Fig. 5. Stars located on the dashed line show no change in hardness between quiescent and flare state.

stellar age. As a consequence, the spectral hardness and the flare luminosity are correlated. The relation between hardness ratios and  $L_F$  is displayed in Fig. 12 and suggests that the more luminous flares are associated with hotter plasma.

## 9. Discussion

### 9.1. Methods for flare detection

Using binned data to detect flares introduces observational restrictions. The sensitivity for detection of small flares is lower and very short flares remain unobserved due to the time binning. Apart from these limitations, our flare detection produces reliable results as verified by comparison to both an alternative approach using Bayesian statistics and, where possible, previous detections of flares by visual inspection stated in the literature.

The importance of Bayesian statistics to astronomical time series analysis has been described by Scargle (1998) and first applied to *ROSAT* observations of flare stars by Hambaryan et al. (1999). This approach, unlike the ‘classical’ method used here, works on the raw, unbinned data and therefore has a time resolution which is only limited by the instrument clock.

We have performed a detailed comparison of the events recognized by the two methods. For the flare detection with the Bayesian algorithm the prior odds ratio,  $O_{\text{pri}}$ , was set to 1. This

	<i>HR 1</i>		
	Quiescence	Rise	Decay
TTS	$0.75 \pm 0.38$	$0.54 \pm 0.47$	$0.70 \pm 0.44$
Pleiads	$0.54 \pm 0.26$	$0.50 \pm 0.29$	$0.58 \pm 0.30$
Hyads	$-0.09 \pm 0.24$	$-0.16 \pm 0.15$	$-0.07 \pm 0.16$
	<i>HR 2</i>		
	Quiescence	Rise	Decay
TTS	$0.36 \pm 0.24$	$0.38 \pm 0.31$	$0.39 \pm 0.21$
Pleiads	$0.07 \pm 0.20$	$0.08 \pm 0.22$	$0.21 \pm 0.14$
Hyads	$-0.01 \pm 0.12$	$-0.04 \pm 0.27$	$0.14 \pm 0.27$

**Table 11.** Evolution of the *ROSAT* PSPC hardness ratios *HR 1* and *HR 2* during stellar flares. Given are the weighted means of flares on TTSs, Pleiads, and Hyads measured during three different phases selected from the X-ray lightcurve: Quiescence (pre- and post-flare), Rise, and Decay. A slight increase in hardness is observed between quiescence and rise phase, but is not significant due to the large spread of the data within one sample. During the decay the spectrum retains its hardness. This indicates additional heating taking place during the decay phase. For each of the flare stages the spectral hardness decreases from TTSs over Pleiads to Hyads.

means that at the beginning one-rate and two-rate Poisson pro-

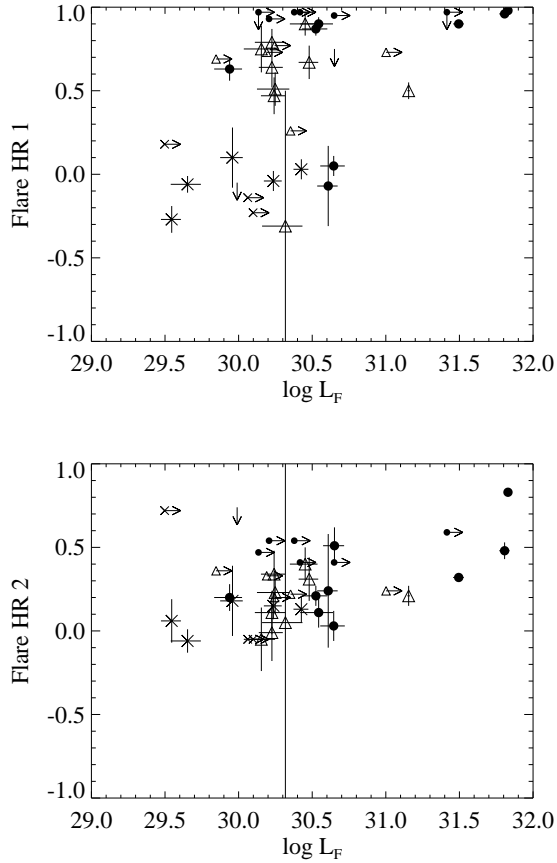


**Fig. 12.** Correlation between *ROSAT* PSPC hardness ratios and flare luminosity  $L_F$ . The meaning of the plotting symbols is the same as in Fig. 11. Lower limits for  $L_F$  are shown when a data gap precedes the observed maximum of the lightcurve (see Tables 3, 4 and 5)

cesses are assumed to have the same probability for being the correct description of the data set. The significance of any detection of variability is then given by the value of the posterior odds ratio,  $O_{21}$ . Applied to our data, 62 events are found at the  $5\sigma$  level, and 95 events have  $O_{21}$  corresponding to at least  $3\sigma$ . All but 5 of the flares discussed in this paper were among the  $5\sigma$  detections. The remaining ones are detected at  $> 3\sigma$ . But note that with the Bayesian method we find variability in 182 lightcurves (in contrast to our 52 flares).

Although the Bayesian approach is sensitive to short events, we have persisted on the criteria explained in Sect. 4.1 for two reasons: (i) While Bayesian statistics are sensitive to all kinds of temporal variability, we are here interested in large flare events only. This makes an additional selection process necessary. (ii) Comparison with the classical flare search used in this paper has shown that the Bayesian method needs further refinement. E.g. the outcome of the present algorithm used to search for flares depends sensitively on the value of the prior odds ratio.

## 9.2. Interpretation of the results

Before flares on different stellar groups are compared, it must be checked whether the composition of these samples is similar. The X-ray luminosity of MS stars depends on their spectral type. Therefore it would be desirable to separately investigate the flare activity from stars of different spectral types. However this is hindered by the low flare statistics. We have performed statistical tests where the flaring TTSs, Pleiads, and Hyads have been compared regarding to their  $T_{\text{eff}}$  and hence spectral types. These tests have shown that it is justified to jointly analyse flares on all late-type stars, i.e. stars with spectral type G, K, and M.

We have shown that the relative number of flares increases when going from spectral types G to K (see Fig. 7). Hereby, we have taken into account that the detection sensitivity for flares depends on the level of measured quiescent emission and hence on the spectral type. An interpretation is that deeper convection zones are favorable to the occurrence of surface flares.

### 9.2.1. Age

We found that in terms of absolute flare luminosity and energy output TTSs surpass both Pleiads and Hyads. The mean flare luminosity of TTSs ( $L_{F,\text{TTS}} = 1.13 \cdot 10^{31}$  erg/s) is almost an order of magnitude higher than that for Hyads ( $L_{F,\text{Hya}} = 1.15 \cdot 10^{30}$  erg/s). The mean Pleiades flare luminosity is intermediate between that for TTSs and Hyades stars with  $L_{F,\text{Ple}} = 3.26 \cdot 10^{30}$  erg/s (see also Fig. 5 and Table 8). This is partly due to the different distances of our stellar samples which result in different detection sensitivities for flares. Note, however, that this effect can explain only why no events with small  $L_F$  are observed on TTSs. But the lack of large events on Hyades stars is real. In Sect. 7 flare rates for TTSs, Pleiads, and Hyads have been established from an evaluation of the observed flare durations and the total observing time. Both, flare rate and mean flare luminosity decline with increasing stellar age.

The quiescent luminosity of Hyades stars which showed a flare is larger than the average  $L_{\text{qui}}$  of Hyads (see Sect. 6.2). More than 90% of the detected Hyades stars are bright enough for detection of an average Hyades flare. Therefore, this result is not a selection effect, and we can conclude that only the most X-ray luminous Hyades stars exhibit X-ray flares. The interesting question whether the enhanced X-ray luminosity of flaring Hyades stars can be explained by their rotation rate can not be pursued with this set of data, because only for half of the flaring Hyades stars measurements of  $v \sin i$  are available.

### 9.2.2. Circumstellar Envelope

If magnetic interactions between star and disk take place, the field lines will constantly become twisted by differential rotation (Montmerle et al. 2000). This may provide an environment favorable for magnetic reconnection and related flare activity.

Six of the observed flare events can be attributed to cTTSs and 8 events to wTTSs. One of the flares on TTSs occurred ei-

ther on DD Tau, a cTTS, or on CZ Tau, a wTTS, both of which are not resolved in the *ROSAT* PSPC observations. Two-sample tests show clear indications that flares on cTTSs are more X-ray luminous than those on wTTSs (see Table 7). This holds no matter on which side the ambiguous event is counted. The flare rate is also slightly higher for cTTSs than for wTTSs, however with low significance. Given the fact that quiescent X-ray emission of wTTSs is stronger than in cTTSs, this observation is surprising. A possible interpretation is that the stronger flare events on cTTSs may be due to violent interaction with their disks.

### 9.2.3. Multiple Flares

During four observations a second flare followed the first one (see lightcurves of VA 334, VB 141, RXJ 0437.5+1851B, and T Tau in Figs. 2 and 4). From the number of observed flares and the total observing time the average duration between two flare events is estimated to be  $> 100$  h. Therefore, from a statistical point of view it is very unlikely to observe so many unrelated ‘double events’. We note, that double flares have been reported in the optical. And Guenther & Ball (1999) have presented two flares that occurred within a few hours from the wTTS V819 Tau.

A possible interpretation of multiple flares is the star-disk scenario proposed by Montmerle et al. (2000) and mentioned in the previous subsection. However, this model does not seem to be accurate for our objects, which are more evolved and in part are known not to possess disks.

### 9.2.4. Projected Rotational Velocity

The statistical tests we have performed to discriminate between slow and fast rotators (with boundary drawn at 20 km/s) reveal no dependence of individual flare parameters  $L_F$ ,  $L_{\text{qui}}$ ,  $\tau_{\text{dec}}$ , and  $L_F/L_{\text{qui}}$  on the rotation rate. However, the flare frequency is about three times higher for fast rotators as compared to slow rotators:  $F_{\text{slow}} = 0.55 \pm 0.10\%$  and  $F_{\text{fast}} = 1.55 \pm 0.38\%$ .

### 9.2.5. Binary Interactions

We have searched for evidence of binary interaction during X-ray flares by dividing our sample of flares into spectroscopic binaries and all other systems, i.e. wide (or visual) multiples and single stars, in which such interactions can not take place. The comparison of flare rates  $F$  showed that large X-ray flares are significantly more frequent on spectroscopic binaries:  $F_{\text{SB}} = 1.43 \pm 0.25\%$  and  $F_{\text{non-SB}} = 0.64 \pm 0.12\%$ . We have taken account of all components in multiple systems when evaluating the flare rate. Therefore, the difference in  $F$  between close binaries and other stars seems indeed to indicate that magnetic interactions within close binaries leads to increased flare activity. But note, that interbinary events are expected to have longer durations because of the larger scale of the magnetic configuration. Our statistical observations did not show an increase of the time scales for spectroscopic binaries.

### 9.2.6. Spectral signatures during flares

From the lower panels of Fig. 11 it can be concluded that for most of the observed events the spectral hardness has increased during the flare. Due to the large uncertainties, however, the changes in the mean hardness are only marginal. But, note, that the uncertainties represent the standard deviation (computed by taking into account upper/lower limits to the hardness) and thus reproduce the spread in the data.

We think that the X-ray emission of TTSs is harder than that of Pleiades and Hyades stars (see Table 11) for two reasons: (i) Because of their circumstellar envelope TTSs suffer from much stronger absorption than Pleiads and Hyads, and absorption is stronger for Pleiads than for Hyads due to the larger distance of the former, (ii) the younger the stars, the stronger the activity, and therefore the harder the spectrum.

## 10. Conclusions

We have determined flare rates for PMS stars, Pleiades and Hyades on a large data set and found that all stars are observed during flares for less than 1% of the observing time. Both frequency and strength of large X-ray flares decline after the PMS phase.

To probe whether the activity changes in the presence of a circumstellar disk, e.g. as a result of magnetic interactions between the star and the disk, we have compared flares on cTTSs and wTTSs. We find that flares on cTTSs are stronger and more frequent.

A comparison of flares on spectroscopic binaries to flares on all other stars of our sample shows that the flare rate is by a factor of  $\sim 2$  higher for the close binaries.

The flare rate of fast rotators is enhanced by a factor of  $\sim 3$  as compared to slowly rotating stars.

To summarize, our analysis confirms that age and rotation influence the magnetic activity of late-type stars. All previous studies in this field have focused on the quiescent X-ray emission. Now, for the first time the rotation-activity-age connection has been examined for X-ray flares. Furthermore, from the sample of flares investigated here we find evidence that magnetic activity goes beyond solar-type coronal activity: On young stars interactions between the star and a circumstellar disk or the magnetic fields of close binary stars may play a role.

*Acknowledgements.* We made use of the Open Cluster Database, compiled by C.F. Prosser and J.R. Stauffer. We thank S. Wolk and W. Brandner for useful discussions and an anonymous referee for valuable comments. RN acknowledges grants from the Deutsche Forschungsgemeinschaft (Schwerpunktprogramm ‘Physics of star formation’). The *ROSAT* project is supported by the Max-Planck-Gesellschaft and Germany’s federal government (BMBF/DLR).

## References

- Anderson C. M., Stöckly R., Kraft R. P., 1966, ApJ 143, 299  
 Beckwith S. V. W., Sargent A. I., Chini R. S., Güsten R. 1990, AJ 99, 924

- Bertout C., Basri G., Bouvier J. 1988, *ApJ* 330, 350
- Bouvier J., Cabrit S., Fernández M., Martín E. L., Matthews J. M. 1993, *A&A* 272, 176
- Bouvier J., Forestini M., Allain S. 1997a, *A&A* 326, 1023
- Bouvier J., Rigaut F., Nadeau D. 1997b, *A&A* 323, 139
- Briceño C., Hartmann L., Stauffer J., Martín E. 1998, *AJ* 115, 2074
- Caillault J.-P., 1996, In: Pallavicini R. and Dupree A. K. (eds.), *Cool Stars, Stellar Systems, and the Sun*, 9th Cambridge Workshop, ASP Conf. Ser., Vol.109, 325
- Cernicharo J., Bachiller R., Duvert G., 1985, *A&A* 149, 273
- Cohen M., Kuhl L. V. 1979, *ApJS* 41, 743
- Cruddace R. G., Hasinger G. R., Schmitt J. H. M. M., 1988, In: Murtagh F., Heck A. (eds.) *Astronomy from large databases*, ESO, Garching, p.177
- Elias J. H., 1978, *ApJ* 224, 857
- Feigelson E. D., DeCampli W. M. 1981, *ApJ* 243, L89
- Feigelson E. D., Nelson P. I. 1985, *ApJ* 293, 192
- Gagné M., Caillault J.-P. 1994, *ApJ* 437, 361
- Gagné M., Caillault J.-P., Stauffer J. R., 1995, *ApJ* 450, 217
- Ghez A. M., Neugebauer G., Matthews K. 1993, *AJ* 106, 2005
- Gizis J. E., Reid I. N. 1999, *AJ* 117, 508
- Grosso N., Montmerle T., Feigelson E. D., André P., Casanova S., Gregorio-Hetem J. 1997, *Nat* 387, 56
- Griffin R. F., Gunn J. E., Zimmerman B. A., Griffin R. E. M. 1985, *AJ* 90, 609
- Guenther E. W., Ball M. 1999, *A&A* 347, 508
- Guenther E. W., Lehmann H., Emerson J. P., Staude J. 1999, *A&A* 341, 768
- Hambaryan V., Neuhäuser R., Stelzer B. 1999, *A&A* 345, 121
- Haro G., Chavira E., Gonzalez G., 1982a, Instituto de Tonantzintla, Boletín Vol.3, 3
- Hartmann L., Stauffer J. R., 1989, *AJ* 97, 873
- Hearty T. J., Neuhäuser R., Stelzer B., Fernández M., Alcalá J. M., Covino E., et al. 2000, *A&A*, in press
- Herbig G. H. 1998, *ApJ* 497, 736
- Herbig G. H., Bell K. R., 1988, *Lick Observatory Bulletin*, No. 1111
- Hertzsprung E. 1947, *Ann. Leiden Obs.* 19, No. 1A
- Hodgkin S. T., Jameson R. F., Steele I. A., 1995, *MNRAS* 274, 869
- Johnson H. L., Mitchell R. I., 1958, *ApJ* 128, 31
- Jones B. F., Fischer D. A., Stauffer J. R. 1996, *AJ* 112, 1562
- Kenyon S. J., Hartmann L., 1995, *ApJS* 101, 117
- Köhler R., Leinert Ch. 1998, *A&A* 331, 977
- Kraft R. P. 1965, *ApJ* 142, 681
- Leinert Ch., Zinnecker H., Weitzel N., et al. 1993, *A&A* 278, 129
- Li J. Z., Hu J. Y., 1998, *A&AS* 132, 173
- Luhman K. L. 1999, *ApJ* 525, 466
- Luyten W. J., Hill G., Morris S. 1981, *Proper Motion Survey*, Minneapolis, Univ. of Minnesota
- Magazzù A., Martín E. L., Sterzik M. F., Neuhäuser R., Covino E., Alcalá J. M. 1997, *A&AS* 124, 449
- Martín E. L., Magazzù A. 1999, *A&A* 342, 173
- McCaughrean M. J., O'Dell C. R. 1996, *AJ* 111, 1977
- Mendoza V E. E. 1956, *ApJ* 123, 54
- Mermilliod J. C., Turon C., Robichon N., Arenou F., Lebreton Y. 1997, In: Battrick B. (ed.), *ESA Symposium 'Hipparcos Venice '97'*, Venice, Italy, ESA SP-402, 643
- Mewe R., Gronenschild E. H. B. M., van den Oord G. H. J., 1985, *A&AS* 62, 197
- Mewe R., Lemen J. R., van den Oord G. H. J., 1986, *A&AS* 65, 511
- Micela G., Sciortino S., Kashyap V., Harnden Jr. F. R., Rosner R. 1996, *ApJS* 102, 75
- Micela G., Sciortino S., Harnden Jr. F. R., et al. 1999, *A&A* 341, 751
- Montmerle T., Koch-Miramond L., Falgarone E., Grindlay J. E. 1983, *ApJ* 269, 182
- Montmerle T., Grosso N., Tsuboi Y., Koyama K., 2000, *ApJ* in press
- Morel M., Magnenat P. 1978, *A&AS* 34, 477
- Morgan W. W., Hiltner W. A. 1965, *ApJ* 141, 177
- Neuhäuser R., 1997, *Science* 276, 1363
- Neuhäuser R., Sterzik M. F., Schmitt J. H. M. M., Wichmann R., Krautter J. 1995, *A&A* 297, 391
- Neuhäuser R., Torres G., Sterzik M. F., Randich S. 1997, *A&A* 325, 647
- Neuhäuser R., Briceño C., Comerón F., et al. 1999, *A&A* 343, 883
- Oppenheimer B. R., Basri G., Nakajima T., Kulkarni S. R. 1997, *AJ* 113, 296
- Pallavicini R., Golub L., Rosner R., Vaiana G. S., Ayres T., Linsky J. L. 1981, *ApJ* 248, 279
- Panzera M. R., Tagliaferri G., Pasinetti L., Antonello E. 1999, *A&A* 348, 161
- Perryman M. A. C., Brown A. G. A., Lebreton Y., et al. 1998, *A&A* 331, 81
- Pesch P. 1968, *ApJ* 151, 605
- Preibisch T., 1997, *A&A* 324, 690
- Preibisch T., Zinnecker H., Schmitt J. H. M. M., 1993, *A&A* 279, L33
- Preibisch T., Neuhäuser R., Alcalá J. M., 1995, *A&A* 304, L13
- Preibisch T., Zinnecker H., Herbig G. H., 1996, *A&A* 310, 456
- Prosser C. F., Stauffer J. R., Kraft R. P. 1991, *AJ* 101, 1361
- Pye J. P., Hodgkin S. T., Stern R. A., Stauffer J. R., 1994, *MNRAS* 266, 798
- Queloz D., Allain S., Mermilliod J.-C., Bouvier J., Mayor M. 1998, *A&A* 335, 183
- Raboud D., Mermilliod J.-C. 1998, *A&A* 329, 101
- Reid I. N., Hawley S. L., 1999, *AJ* 117, 343
- Raymond J. C., Smith B. W., 1977, *ApJS* 35, 419
- Scargle J. D., 1998, *ApJ* 504, 405
- Schmitt J. H. M. M., Favata F., 1999, *Nat* 401, 44
- Schmidt-Kaler, T. H. 1982, *Physical Parameters of Stars*, in: Landolt-Bornstein New Series, Vol 2b, *Astronomy and Astrophysics Stars and Star Clusters* (eds. K. Shaifers & H. H. Voigt), New York, Springer
- Skinner S. L., Güdel M., Koyama K., Yamauchi S. 1997, *ApJ* 486, 886

- Soderblom D. R., Jones B. F., Balachandran S., et al. 1993a, *AJ* 106, 1059
- Soderblom D. R., Stauffer J. R., Hudon J. D., Jones B. F. 1993b, *ApJS* 85, 315
- Stauffer J. R. 1982, *AJ* 87, 1507
- Stauffer J. R. 1984, *ApJ* 280, 189
- Stauffer J. R., Hartmann L. W., Soderblom D. R., Burnham N. 1984, *ApJ* 280, 202
- Stauffer J. R., Hartmann L. W., 1987, *ApJ* 318, 337
- Stauffer J. R., Hartmann L. W., Latham D. W. 1987, *ApJ* 320, L51
- Stauffer J. R., Klemola A., Prosser C., Probst R. 1991, *AJ* 101, 980
- Stauffer J. R., Caillault, J.-P., Gagné M., Prosser C., Hartmann L. W. 1994, *ApJS* 91, 625
- Stauffer J. R., Balachandran S. C., Krishnamurthi A., Pinsonneault M., Terndrup D. M., Stern R. A. 1997, *ApJ* 475, 604
- Stefanik H. P., Latham D. W. 1992, 'Binaries in the Hyades', In: 'Complementary Approaches to Double and Multiple Star Research', IAU Colloq. 135, ASP Conf. Ser. 32, (McAlister H. A. & Hartkopf W. I., eds.), p. 173
- Stern R. A., Schmitt J. H. M. M., Pye J. P., Hodgkin S. T., Stauffer J. R., Simon T. 1994, *ApJ* 427, 808
- Strom K. M., Strom S. E., 1994, *ApJ* 424, 237
- Strom K. M., Strom S. E., Edwards S., Cabrit S., Skrutskie M. F. 1989, *AJ* 97, 1451
- Tsuboi Y., Koyama K., Murakami H., Hayashi M., Skinner S., Ueno S. 1998, *ApJ* 503, 894
- Torres C. A. O., Quast G., de la Reza R., Gregorio-Hetem J., Lépine J. R. D. 1995, *AJ* 109, 2146
- van Altena W. F. 1969, *AJ* 74, 2
- van Bueren H. G. 1952, *Bull. Astron. Inst. Netherlands*, 11, 385
- Walter F. M. 1983, *ApJ* 274, 794
- Walter F. M., Brown A., Linsky J. L., et al. 1987, *ApJ* 314, 297
- Wichmann R., Krautter J., Schmitt J. H. M. M., Neuhäuser R., Alcalá J. M., Zinnecker H., et al. 1996, *A&A* 312, 439
- Wichmann R., Bastian U., Krautter J., Jankovics I., Ruciński S. M. 1998, *MNRAS* 301, L39
- Zickgraf F.-J., Alcalá J. M., Krautter J., Sterzik M. F., Appenzeller I., Motch C., et al. 1998, *A&A* 339, 457
- Ziskin V. 1993, Senior Thesis, Harvard University